

1 **The value of water isotope data on improving process**
2 **understanding in a glacierized catchment on the Tibetan**
3 **Plateau**

4 Yi Nan¹, Lide Tian^{2,3}, Zhihua He⁴, Fuqiang Tian¹, Lili Shao²

5 ¹Department of Hydraulic Engineering, State Key Laboratory of Hydroscience and Engineering,
6 Tsinghua University, Beijing 100084, China

7 ²Institute of International Rivers and Eco-security, Yunnan University, Kunming, China

8 ³CAS Center of Excellence in Tibetan Plateau Earth Sciences, Beijing 100101, China

9 ⁴Center for Hydrology, University of Saskatchewan, Saskatchewan, Canada

10 ***Corresponding to:*** Fuqiang Tian

11 Address: Room 330 New Hydraulic Building, Tsinghua University, Beijing 100084, China

12 Email: tianfq@mail.tsinghua.edu.cn

13 **Abstract**

14 This study integrated a water isotope module into the hydrological model THREW which has been
15 successfully used in high and cold regions. Signatures of oxygen stable isotope (^{18}O) of different water
16 inputs and stores were simulated coupling with the simulations of runoff generations. Isotope
17 measurements of precipitation water samples and ~~global precipitation isotope product, as well as~~ assumed
18 constant isotope signature of ice meltwater were used to force the isotope module. Isotope signatures of
19 water stores such as snowpack and subsurface water were updated by an assumed completely mixing
20 procedure. Fractionation effects of snowmelt and evapotranspiration were modeled in a Rayleigh
21 fractionation approach. The isotope-aided model was subsequently applied for the quantifications of
22 runoff components and estimations of mean water travel time (MTT) and mean residence time (MRT) in
23 the glacierized watershed of Karuxung River on the Tibetan Plateau. Model parameters were calibrated
24 by three variants with different combinations of observations including streamflow, snow cover area and
25 isotopic composition of stream water. ~~Model parameters were constrained by three different~~
26 ~~combinations of observations including a single objective calibration using streamflow measurement~~
27 ~~solely, a dual objective calibration using both streamflow measurement and MODIS estimated snow~~
28 ~~cover area, and a triple objective calibration using additionally isotopic composition of stream water.~~
29 Modeled MTT and MRT was validated by estimate of a tracer-based sine-wave method. Results indicate
30 that: (1) the proposed model performed performs quite well on simultaneously reproducing the
31 observations of streamflow, snow cover area, and isotopic composition of stream water, despite that only
32 precipitation water samples were available for tracer input; (2) isotope data helped to facilitate more
33 estimate more plausible robust estimations on contributions of runoff components (CRCs) to streamflow
34 in the melting season, as well as on, and improved the robustness of MTT and MRT estimations; (3)
35 involving isotope data for the model calibration obviously reduced reduces uncertainties of the
36 quantification of CRCs and estimations of MTT and MRT, through better constraining the ~~strong~~
37 competitions among different runoff processes induced by meltwater and rainfall. Our results inform
38 high value of water isotope data on improving process understanding in a glacierized basin on the Tibetan
39 Plateau.

40 **Keywords:**

41 Tracer-aided hydrological model; Contribution of runoff components; Water travel time; Glacierized
42 catchment; Tibetan Plateau

43

44

45 **1. Introduction**

46 Glacierized catchments in mountainous regions are generally headwater catchments, which are of
47 great interest because of its complex runoff generation processes and important role on supplying water
48 sources for downstream regions (Immerzeel et al., 2010). Stable isotopes in water ($\delta^2\text{H}$ and $\delta^{18}\text{O}$) are
49 powerful tools for investigating the water cycle and hydrological processes (Gat, 1996; Bowen et al.,
50 2019). Isotopic composition of water changes with multiple ecological and hydrological processes, and
51 is affected by several environmental factors (Zhao et al., 2012; Wang et al., 2013), thus is frequently used
52 to track the storage and transportation of water. Isotopic compositions generally distinguish among
53 different water bodies and phases (Xi, 2014), thus is widely used to determine the relative dominance of
54 water sources, especially in the glacierized catchments (Kong et al., 2019; He et al., 2020). Water isotope
55 data consequently bears the potential on improving the understanding of hydrological processes in
56 glacierized catchments.

57 The Tibetan Plateau as a high mountainous cryosphere is the source of many major rivers in Asia
58 including Yarlung Tsangpo-Brahmaputra River, Ganges River, Indus River and so on (Report of STEP,
59 2018). Scientific understanding of hydrological processes in this region is critical in predicting the
60 responses of water resources and water hazards to climate changes (Lutz et al., 2014; Immerzeel et al.,
61 2010; Miller et al., 2012). River runoff in these basins is prominently fed by multiple water sources
62 including snowmelt, glacier melt and rainfall (Li Zongxing et al., 2019). Coupling with the strong spatio-
63 temporal variabilities of meteorological inputs, the complicated runoff generation processes imply big
64 challenges in understanding the hydrological behaviors in glacierized basins on the Tibetan Plateau.

65 It is, therefore, of critical importance to quantify contributions of runoff components (CRCs) to
66 streamflow in glacierized regions. Estimating CRCs by hydrological models is one of the commonly
67 adopted method (Weiler et al. 2018), which is particularly subject to the following challenges. First,
68 modeled CRCs rely heavily on the model conceptualizations of the mixing and propagations of different
69 water sources in the basin. Model configurations and corresponding parameters representing the storage
70 capacities of soil layers and groundwater aquifers obviously affect the relative proportions of surface and
71 subsurface flow to streamflow (Nepal et al. 2014). CRCs modeled by different hydrological models are
72 thus rarely comparable (Tian et al. 2020). For example, Nepal et al. (2015) and Siderius et al. (2013)
73 compared CRCs estimated by different glacio-hydrological models in glacierized basins in the
74 Himalayan region, and demonstrated considerable variations of the modeled CRCs. They attributed the
75 difference to the variations of the model conceptualizations. Second, strong compensatory effects of the
76 simulated runoff induced by precipitation and ice meltwater which were typically not well constrained
77 in the model resulted in large variations of the modeled CRCs. For instance, modeling results from
78 Duethmann et al. (2015) and Finger et al. (2015) indicated that overestimated precipitation-triggered
79 runoff in the model can be easily compensated by an underestimated ice melt runoff and vice versa,
80 especially in high altitude glacierized basins where precipitation input have large uncertainty.

81 Tracer data of water stable isotope have been widely used to label runoff components in the popular
82 end-member mixing approach (e. g., Kong et al. 2011; He et al. 2020). Its value for improving modeled
83 CRCs, however, have not been sufficiently investigated. Previous applications of tracer-aided
84 hydrological models which integrated the simulation of water isotopic compositions of different runoff
85 components into the rainfall/melting-runoff processes in snow dominated basins have demonstrated high
86 values of water isotope data on diagnostically improving model structure and recognizing the dominances
87 of runoff processes on streamflow (Capell et al., 2012; Delavau et al. 2017; Son and Sivapalan, 2007;

88 Birkel et al., 2011; Stadnyk and Holmes, 2020). An early test of the isotope-aided hydrological model in
89 a glacierized basin in Tianshan Central Asia of He et al. (2019) indicated that additionally use of isotope
90 data helped to constrain the internal apportionments of runoff components in the model and improved
91 the estimation of CRCs at an event scale. However, exploring the values of water isotope data for
92 hydrological modelling in glacierized basins are still limited to the low availability of water tracer data
93 from field water sampling due to the harsh environment, especially for glacierized basins on the Tibetan
94 Plateau. As far as we know, glacio-hydrological model coupled with the simulations of isotope signatures
95 have not been developed and tested in the Tibetan Plateau yet.

96 Quantifying the time from entrance of water to its exits is fundamental to understandings of flow
97 pathways and the storage and mixing processes (McGurie and McDonnell, 2006). Characterizing water
98 travel time distribution (TTD) and mean travel time (MTT) in addition to the traditional focus on
99 streamflow response allows us to be closer to getting the right answers for the right reasons (Hrachowitz
100 et al. 2013). Despite that TTD and MTT serve good tools to diagnose unsuitable model structures and
101 parameterizations (McMillan et al. 2012), it has been rarely quantified in glacierized basins. Plenty of
102 convenient tools have been developed based on lumped parameter models, but their practical applications
103 in glacierized basins are restricted by the time invariant assumption and the weakness on considering the
104 strong spatio-temporal variability of runoff processes (van Huijgevoort et al. 2016) as well as the seasonal
105 water inputs from snowmelt and glacier melt. Fully physically-based water particle tracking approaches
106 coupling with hydrological processes whereas are only limited to small basins due to the heavy
107 computation cost (Remondi et al. 2018). Conceptual models that used additional tracer storage
108 compartments along with the flow and transport processes have provided crucial information on the
109 dynamics of flow pathways and storages, but rely heavily on the prior definitions of function shape (e.g.,
110 travel time distribution (TTD) in van der Velde et al. 2015; StorAge Selection function (SAS) in Benettin
111 and Bertuzzo 2018; age-ranked storage-discharge relation in Harman 2019). In contrast, tracer-aided
112 hydrological models that integrated the storage and transportation of conservative water tracers into the
113 runoff generation processes have been demonstrated as successful on estimating TTD and water ages as
114 well as their time variances with in snowmelt influenced basins (e.g., Soulsby et al. 2015; Ala-Aho et
115 al.2017). However, such hydrological models have not been applied in glacierized basins for estimations
116 of TTD and MTT yet.

117 For process understanding in glacierized basins, glacio-hydrological models that additionally
118 represented the snow processes and glacier evolution have been widely used (e.g, Immerzee et al. 2013;
119 Lutz et al. 2014 and 2016; Luo et al. 2018). The more complex integration of water sources from different
120 flow pathways and units whereas resulted in expanded parameter space of these hydrological models
121 which introduced large uncertainty in the model calibration (Finger et al. 2015). Equifinality is serious
122 in these regions when calibrating hydrological model by streamflow solely, indicating that different
123 parameters and runoff component proportions could perform similarly in discharge simulation (Beven
124 and Freer, 2001; Chen et al., 2017), despite of the general good performance for streamflow simulation.
125 Therefore, multiple datasets including glacier observation and remotely sensed snow products have been
126 frequently used in addition to streamflow measurements in vast glacio-hydrological simulations (e.g.,
127 Parajka and Blöschl, 2008; Konz and Seibert, 2010; Schaeffli and Huss 2011; Duethmann et al. 2014;
128 Finger et al., 2015; He et al. 2018). However, both discharge and snow/glacier measurements provide
129 insufficient constraints on distributions of flow pathways and the parameterizations of subsurface water
130 storages (He et al. 2019). Although application in a glacierized basin in Central Asia of He et al. (2019)
131 indicated high utility of isotope data on constraining the complex interactions of multiple runoff

132 processes for the quantifications of CRCs, the values of water tracer such as stable isotope on reducing
133 uncertainties on the estimations of TTD and MTT in glacierized basins on Tibetan Plateau have not been
134 investigated.

135 In light of those backgrounds, this study integrated the simulation of oxygen isotope signatures into
136 a hydrological model that has been proved effective to simulate the runoff processes on the Tibetan
137 Plateau. The developed tracer-aided hydrological model was applied to the Karuxung River catchment
138 (286 km², 4550 to 7206 m a.s.l.) on Tibetan Plateau. The objectives of this study are: (1) to test the
139 capability of the proposed tracer-aided model on simultaneously reproducing streamflow and isotope
140 signatures of stream water in the study basin where only precipitation water samples are available for
141 isotope input, (2) to evaluate the values of tracer-aided method on improving the estimation of CRCs and
142 TTD/MTT in the study basin, and (3) to assess and interpret the differences between modeled TTD/MTT
143 and estimates by a lumped parameter method.

144 2. Materials and methodology

145 2.1 Study area and data

146 This study focuses on the Karuxung catchment, which is located in the upper region of the Yarlung
147 Tsangpo River basin, on the northern slope of the Himalayan Mountains (Figure 1). Digital elevation
148 model (DEM) data in the study catchment with a spatial resolution of 30-m was downloaded from the
149 Geospatial Data Cloud (www.gscloud.cn). The Karuxung river originates from the Lejin Jangsan Peak
150 of the Karola Mountain at 7206 m above sea level (a.s.l.), and flows into the Yamdrok Lake at 4550m
151 a.s.l. (Zhang et al., 2006). The catchment covers an area of 286 km². The river discharge is significantly
152 influenced by the headwater glaciers which cover an area of around 58 km² (Mi et al., 2001). This
153 catchment is dominated by a semi-arid climate. The mean annual temperature and precipitation at
154 Langkazi Weather Station were 3.4°C and 379 mm, respectively. Due to the effect of the South Asian
155 Monsoon, more than 90% of the annual precipitation falls between June and September. Precipitation
156 occurs mostly in form of snow from October to the following March at high elevations (Zhang et al.,
157 2015).

158 [Figure 1]

159 Daily temperature and precipitation data from 1st January 2006 to 30th September 2012 were
160 collected at the Langkazi Weather Station (4432 m a.s.l.). Altitudinal distributions of temperature and
161 precipitation across the catchment were estimated by the lapse rates reported in Zhang et al. (2015).
162 Runoff were measured daily from 1st April 2006 to 31st December 2012 at the Wengguo Hydrological
163 Station at the catchment outlet. The coverages of glaciers were extracted from the Second Glacier
164 Inventory Dataset of China (Liu, 2012). The 8-day snow cover extent data from MODIS product of
165 MOD10A2 (500m×500m, Hall and Riggs, 2016) were used to denote the fluctuations of the snow cover
166 area (SCA). The 8-day Leaf Area Index (LAI) and the monthly normalized difference vegetation index
167 (NDVI) data were downloaded from MODIS product of MOD15A2H (500m×500m, Myneni et al., 2015)
168 and MOD13A3 (1km×1km, Didan, 2015). Soil hydraulic parameters were estimated based on the soil
169 properties extracted from the 1km × 1km Harmonized World Soil Database (HWSD,
170 <http://www.fao.org/geonetwork/>).

171 Grab samples of precipitation and stream water were collected at the Wengguo Station in 2006-
172 2007 and 2010-2012, for analysis of δ¹⁸O and δ²H, and the characteristics of samples are summarized in

173 Table1. In the dry seasons when precipitation water was not sampled due to small event amounts,
 174 precipitation isotope data from monthly Regionalized Cluster-based Water Isotope Prediction (RCWIP
 175 with a pixel size of 10'×10', Terzer et al., 2013) were used as proxy for model input. The effect of
 176 elevation on the isotopic composition of precipitation was estimated using a lapse rate of -0.34‰/100m
 177 based on Liu et al. (2007). The stream water samples were collected weekly every Monday from the river
 178 channel near the Wengguo Station. Isotopic composition of glacier meltwater was assumed to be constant
 179 during the entire study period and the value reported in Gao et al. (2009) was adopted.

180

[Table 1]

181 2.2 Tracer-aided hydrological model

182 The THREW (Tsinghua Representative Elementary Watershed) model was originally developed by
 183 Tian et al. (2006), and has been successfully applied to a wide range of catchments (e.g., Tian et al., 2012;
 184 Yang et al., 2014), including glacierized basins in the Alps, Tianshan, and the Tibet Plateau (He et al.,
 185 2014; 2015; Xu et al., 2019). The THREW model uses the Representative Elementary Watershed (REW)
 186 method for the spatial discretization of catchment, in which the study catchment is divided into REWs
 187 based on the catchment DEM, and then each of the REWs is divided into sub-zones as the basic units for
 188 hydrological simulation. More details of the model set up are given in Tian et al. (2006). In this study,
 189 the Karuxing catchment was divided into 41 REWs.

190 The snowmelt and glacier melt are differentiated according to the glacier coverage data. The
 191 meltwater in non-glacier area is defined as snowmelt, and the meltwater in glacier covered area is defined
 192 as glacier melt, which includes the meltwater of both ice and snow. The two kinds-of-water sources are
 193 assumed to be melt in different rates, as represented by different degree-day factors. Meltwater from
 194 snow and glacier are simulated using a temperature-index method as given in Eqs. (1) and (2):

195

$$M_{SN} = \begin{cases} DDF_{SN} * (T - T_{SN0}) & \text{for } T > T_{SN0} \\ 0 & \text{for } T \leq T_{SN0} \end{cases} \quad - \quad (1)$$

196

$$M_G = \begin{cases} DDF_G * (T - T_{G0}) & \text{for } T > T_{G0} \\ 0 & \text{for } T \leq T_{G0} \end{cases} \quad (2)$$

197

where, the subscripts SN and G represent snow and glacier, respectively. M is the melt amount, T is
 198 temperature and T_0 refers to temperature threshold above which snow/ice starts to melt. DDF is the
 199 degree-day factor, representing the melt rate. Glacier meltwater (M_G) in this study includes both ice melt
 200 and snowmelt on the glacierized area.

201

The fraction of snowfall (P_{SN}) of the total precipitation P is determined by a temperature threshold
 202 T_{SN} in Eq. 3. Snow water equivalent (SWE) of each REW is thus updated by Eq. 4. The snow cover area
 203 (SCA) of the corresponding REW is determined by a SWE threshold value (SWE_0): when the calculated
 204 SWE is higher than SWE_0 , the SCA of this REW is recorded as 1, otherwise the SCA is assumed to be 0
 205 (similarly to Parajka and Blöschl, 2008; Zhang et al., 2015; He et al., 2014). The SCA of the whole study
 206 catchment is calculated as the ratio of the sum of the areas of snow covered REWs to the total catchment
 207 area. Values of T_N and SWE_0 are set based on prior knowledge from Dou et al. (2011), Marques et al.
 208 (2011) and He et al. (2014): $T_{SN} = 2^\circ\text{C}$, $SWE_0 = 20\text{mm}$.

209

$$P_{SN} = \begin{cases} 0 & T \leq T_{SN} \\ P & T > T_{SN} \end{cases} \quad (3)$$

210

$$\frac{dSWE}{dt} = P_{sA} - M_{sA} \quad (4)$$

211

212

213

214

215

Meltwater of ice and snow, and rainfall over the glacier area are assumed to flow directly into the channel near the glacier tongue in form of surface runoff, based on the low permeability of the glacier surface. Snowmelt in the non-glacier area is assumed to generate runoff in a similar way to rainfall (Schaepli et al., 2005). For model simplicity, the evolution of the glacier area is not simulated in the model for the short simulation period of seven years.

216

217

218

219

220

221

222

223

224

225

226

Simulation of $\delta^{18}\text{O}$ of multiple water sources was integrated into the runoff generation processes in the THREW model (hereafter abbreviated as a THREW-t model). The $\delta^{18}\text{O}$ of water sources in each of the sub-zones was assumed to be conservative, meaning that no chemical reactions occurred during the mixing of water sources. We assumed that the isotopic compositions of precipitation and glacier meltwater are linearly dependent on elevation, and used linear gradients reported in Liu et al. (2007) to estimate the initial isotopic compositions of precipitation and glacier meltwater in individual REWs (similarly to He et al. 2019). The isotopic compositions of the snowpack and subsurface water storages were initialized by a “spin-up” running for three hydrological years, assuming the isotopic compositions of water storages would reach steady levels after three years’ running. Isotope composition of event snowfall on the snowpack was assumed to be the same as that of precipitation occurring in the corresponding REW.

227

228

229

The fractionation effects of evaporation on isotope composition of water were estimated by a Rayleigh fractionation method in Eqs. (5) to (7) (Hindshaw et al., 2011; Wolfe et al., 2007; He et al., 2019):

230

$$\delta^{18}O_x' = \delta^{18}O_x * \frac{1-f^{CF(\frac{1}{\alpha}-1)+1}}{1-f} \quad (5)$$

231

$$\ln\alpha = -0.00207 + \frac{-0.4156}{T} + \frac{1137}{T^2} \quad (6)$$

232

$$f = 1 - \frac{w_x'}{w_x} \quad (7)$$

233

234

235

236

where, $\delta^{18}O_x'$ is the isotope composition of the evaporated water, $\delta^{18}O_x$ is the isotope composition of water before evaporation, α is the Rayleigh fractionation factor, $T(K)$ is air temperature in the corresponding catchment unit, CF is a correction factor, and f is the ratio of remaining water volume to the original water volume before evaporation.

237

238

A complete mixing assumption was used for the tracer signatures in each water storage. Consequently, $\delta^{18}\text{O}$ of soil water and groundwater were updated according to the following equation:

239

$$\delta^{18}O_t = \frac{w_o\delta^{18}O_o + \sum w^i\delta^{18}O^i}{w_o + \sum w^i} \quad (8)$$

240

241

242

243

244

where, w_o and $\delta^{18}O_o$ are the water quantity and isotopic composition of the subsurface storages at the prior step, respectively. w^i refers to the infiltration into the soil storage from water source i . For groundwater storage, w^i refers to the seepage from upper soil water. $\delta^{18}O^i$ stands for the isotopic composition of input water source i . The isotope signature of snowpack was simulated similarly as subsurface water storages according to Eq. 8.

245 Stream water in each of the REWs was considered as a mixture of three components including
 246 inflow from the upstream REWs, runoff generated in the current REW, and the water storage in the
 247 river channel. Consequently, the isotopic composition of stream water in each REW ($\delta^{18}O_r$) was
 248 estimated based on the following conservative mixing equation:

$$249 \quad \delta^{18}O_r = \frac{\delta^{18}O_{r0} * w_r + \sum \delta^{18}O_{r,up}^k * I^k + \delta^{18}O_{sur}R_{sur} + \delta^{18}O_{gw}R_{gw}}{w_r + \sum I^k + R_{sur} + R_{gw}} \quad (9)$$

250 where, $\delta^{18}O_{r0}$ is the isotopic composition of stream water and w_r is the water storage in the river
 251 channel at the time step before the mixing of runoff components. $\delta^{18}O_{r,up}^k$ is the isotopic composition
 252 of stream water coming from the upstream REW k , and I^k is the inflow from the corresponding
 253 upstream REW. Subscripts of *sur* and *gw* refer to the surface runoff and subsurface flow from
 254 groundwater outflow generated in the current REW.

255 2.3 Model calibration

256 The physical meaning and value ranges of the calibrated parameters in the THREW-t model are
 257 described in Table 2. Parameter values were optimized using three calibration variants: (1) single-
 258 objective calibration using only the observed discharge at the catchment outlet, (2) dual-objective
 259 calibration using both observed discharge and MODIS SCA estimates, and (3) triple-objective calibration
 260 using observed discharge, MODIS SCA estimates and $\delta^{18}O$ measurements of stream water. Considering
 261 the data availability, we chose April 1st 2006 to December 31st 2010 as the calibration period, and January
 262 1st 2011 to September 30th 2012 as the validation period. For SCA, we used only the MODIS SCA
 263 estimates during the ablation period (1st May to 30th July) of each year for the model calibration, because
 264 simulations of runoff processes are mostly sensitive to the dynamics of snow cover extent in the melting
 265 period (Duethmann et al., 2014). Only the $\delta^{18}O$ measurements of stream water in the rainy season (from
 266 the first rainfall event to the last rainfall event of each year, as shown in Table 1) were used to optimize
 267 the model parameters, because the measured isotope data for precipitation were only available in this
 268 season. We chose the objective functions of Nash Sutcliffe efficiency coefficient (NSE) (Nash and
 269 Sutcliffe, 1970) and mean absolute error (MAE) to optimize the simulations of discharge, SCA and
 270 isotope respectively (Eqs. 12-14).

$$271 \quad NSE_{dis} = 1 - \frac{\sum_{i=1}^n (Q_{o,i} - Q_{s,i})^2}{\sum_{i=1}^n (Q_{o,i} - \overline{Q_o})^2} \quad (10)$$

$$272 \quad MAE_{SCA} = \frac{\sum_{i=1}^n |SCA_{o,i} - SCA_{s,i}|}{n} \quad (11)$$

$$273 \quad MAE_{iso} = \frac{\sum_{i=1}^n |\delta^{18}O_{o,i} - \delta^{18}O_{s,i}|}{n} \quad (12)$$

274 where, n is the total number of observations. Subscripts of *o* and *s* refer to observed and simulated
 275 variables, respectively. $\overline{Q_o}$ is the average value of observed streamflow during the assessing period.

276 An automatic procedure based on the pySOT optimization algorithm developed by Eriksson et al.
 277 (2015) was implemented for all the three calibration variants to identify the behavioral parameters.
 278 pySOT used surrogate model to guide the search for improved solutions, with the advantage of requiring
 279 few function evaluations to find a good solution. An event-driven framework POAP were used for
 280 building and combining asynchronous optimization strategies. The optimization was stopped if a
 281 maximum number of allowed function evaluations was reached, which was set as 3000 in this study. For

282 the single-, dual- and triple-objective calibration variants, NSE_{dis} , $NSE_{dis} - MAE_{SCA}$, $NSE_{dis} - MAE_{SCA} -$
 283 MAE_{iso} were chosen as combined optimization objectives, respectively. The pySOT algorithm was
 284 repeated 150 times for each calibration variant. The 150 final results were further filtered according to
 285 the metric of NSE_{dis} , i.e., only the parameters producing NSE_{dis} higher than a threshold were regarded as
 286 behavioral parameter sets. For single- and dual-objective calibration, the threshold was selected as 0.75.
 287 Considering the trade-off between discharge and isotope simulation, the threshold was chosen as 0.70
 288 for triple-objective calibration. For each calibration variant, the parameter producing highest combined
 289 optimization objective was regarded as the best parameter set.

290

[Table 2]

291

2.43 Quantifications of the contributions of runoff components to streamflow

292

The contributions of individual runoff components to streamflow were quantified based on two
 293 definitions of the runoff components. In the first definition, we quantified the contributions of individual
 294 water sources including rainfall, snow meltwater and glacier meltwater to the total water input, which
 295 were commonly reported in previous quantifications of runoff components on the Tibetan Plateau (Chen
 296 et al., 2017; Zhang et al., 2013). To be noted, the sum of the three water sources should be larger than the
 297 simulated volume of runoff because of the evaporation loss. Thus, contributions quantified in this
 298 definition only refer to the fractions of the water sources in the total water input forcing runoff processes,
 299 rather than the actual contributions of water sources to streamflow at the basin outlet. In the second
 300 definition, runoff components were quantified based on the runoff generation processes including surface
 301 runoff and subsurface flow. Surface runoff consists of runoff triggered by rainfall and meltwater that feed
 302 streamflow through surface paths, and the precipitation occurring in river channel and contributes to
 303 runoff directly. Subsurface flow is the interflow from groundwater outflow.

304

2.54 Estimation of the water travel time and residence time

305

In this study, the water travel time is estimated by three methods, a lumped analytical method and
 306 two distributed model-based methods. A simplified lumped method, sine-wave method (SW) was used
 307 to provide a reference value of mean travel time (MTT) and mean residence time (MRT) in the catchment.
 308 The adopted model-based methods were developed by van Huijgevoort et al. (2016) and Remondi et al.
 309 (2018), which were referred to as mass-mixing method (MM) and flux-tracking method (FT),
 310 respectively. SW method is based on the isotope data of precipitation and stream water. MM and FT
 311 methods were conducted by the tracer-aided hydrological model using behavior parameter values
 312 identified by the calibration scenarios.

313

SW method has a stationarity assumption that a constant flow field gives constant travel time
 314 distribution (TTDs) (van der Velde et al., 2015). It assumes the form of TTD, and derives the MTT
 315 directly from the series isotopic data (McGuire and McDonnell, 2006). Although the assumption is rather
 316 stringent, SW is widely used in the studies when an approximate estimation of MTT is required (e.g.,
 317 Kirchner, 2016; Garvelmann et al., 2017). Here we assumed the form of TTD as the exponential function,
 318 and the MTT can be estimated according to Eqs. 13-14 (McGuire and McDonnell, 2006; Garvelmann et
 319 al., 2017):

320

$$\delta_t = \bar{\delta} + A * \sin\left(\frac{2\pi}{365} * t + \varphi\right) \quad (13)$$

321

$$MTT = \frac{\sqrt{\left(\frac{1}{A_r/A_p}\right)^2 - 1}}{2\pi} \quad (14)$$

322 where, δ_t is the calculated $\delta^{18}\text{O}$ of stream water or precipitation on day t of the year. $\bar{\delta}$ is the mean $\delta^{18}\text{O}$
 323 of stream water or precipitation measured in different seasons. A and φ are parameters controlling the
 324 amplitude and phase lag, and are estimated based on the fitness between the sine-wave curve and the
 325 $\delta^{18}\text{O}$ measurements. Subscripts of r and p in Eq. 14 represent river and precipitation, respectively.

326 MM method was used to estimate the water age of outflow and water storage in the catchment. For
 327 the outflow (e.g., stream water, evaporation), the concept of water age is consistent with the concept of
 328 “travel time conditional on exit time” by Botter et al. (2011), “flux age” by Hrachowitz et al. (2013), and
 329 “backward travel time” by Harman and Kim (2014). For the water storage (e.g., soil water, groundwater,
 330 snowpack), the concept of water age is consistent with the concept of “residence time” by Botter et al.
 331 (2011) and “residence age” by Hrochowitz et al. (2013). MM method regarded the water age as a kind
 332 of tracer, and simulated the “concentration” of this tracer of the water bodies including snowpack, soil
 333 water and stream water (van Huijgevoort et al., 2016; Ala-aho et al., 2017). The “mass” and
 334 “concentration” of the water age were simulated similarly in Eqs. 8-9, by replacing $\delta^{18}\text{O}$ with water age
 335 of the multiple terms. Event precipitation entering the catchment was treated as new water with a
 336 youngest age equaling to the simulation step of model. The glacier meltwater was regarded as very old
 337 water, and a constant age of 1000 days was adapted in this study. Meanwhile, the age of water stored in
 338 snowpack, soil and river channel were assumed to increase with the ongoing simulation time: water age
 339 increased by one day after each model running at a daily step.

340 FT method ran the model multiple times in parallel to track the fate of each precipitation event
 341 separately (Remondi et al., 2018). All days with precipitation were individually labeled and tracked over
 342 the simulation period by adding an artificial tracer to the water amounts which was assumed to not
 343 otherwise exist anywhere. The snow meltwater was tracked from the time when the snow entered the
 344 catchment as solid precipitation (i.e., snowfall), rather than the time when the snowpack melted. Glacier
 345 meltwater was not tracked, because the evolution of glacier was not simulated in the model, and the travel
 346 time of glacier melt as surface runoff was negligible. Similar as MM method, the MTT of glacier melt
 347 runoff was assumed as a constant value as 1000 days. The mixing and transport processes of the tracer
 348 were also simulated similarly in Eqs 8-9 by replacing $\delta^{18}\text{O}$ with the concentration of the artificial tracer.
 349 By summarizing the mass of labeled precipitation in the water storage and stream water, the TTD
 350 conditional on exit time (backward TTD), TTD conditional on injection time (forward TTD) and
 351 residence time distribution (RTD) can be derived.

352 In summary, this study estimated the water travel time and residence time using a lumped method
 353 (SW), and two model-based methods (MM and FT), and the results of three methods were compared to
 354 test the robustness of travel time estimation in this glacierized basin. Specifically, SW method estimated
 355 the MTT of total discharge and the MRT of water storage directly based on the isotopic data in stream
 356 water and precipitation. MM method estimated the water age of stream water and groundwater storage,
 357 representing the daily backward MTT and MRT respectively, and all the 19 behavioral parameter sets of
 358 triple-objective calibration were used to illustrate the uncertainty of MTT. FT method estimated the time-
 359 varying precipitation-triggered TTD and RTD, only using the parameter set producing best metric. To
 360 make the result of FT method comparable to MM method, the glacier melt runoff was also assumed to

361 have MTT (water age) of 1000 days to calculate the MTT of the total runoff generation as the weighted
362 average value of the MTT of precipitation runoff (including rainfall and snowmelt) and glacier melt
363 runoff according to the contribution of water sources. The glacier melt was assumed to only contribute
364 to surface runoff directly and exit the catchment rapidly, thus had no influence on the MRT estimation.

365 3. Results

366 3.1 Model performance on the simulations of discharge and isotopic composition

367 For the calibration period, the single-objective calibration produced good performance for the
368 simulation of discharge, but had an extremely poor performance for the simulations of SCA and $\delta^{18}\text{O}$
369 (Table 3). Involving SCA in the calibration objective, the dual-objective calibration significantly
370 improved the simulation of SCA, and kept a good behavior on discharge simulation, but brought no
371 benefit to the isotope simulation. The triple-objective variant led to a good performance for all the three
372 metrics. The NSE_{dis} produced by triple-objective calibration was slightly lower than that of another two
373 variants because of the lower threshold for behavior parameter sets. The simulation of isotopic
374 composition of stream water was significantly improved by triple-objective calibration compared to the
375 other two variants. For the validation period, the NSE_{dis} of triple-objective calibration was significantly
376 improved, even better than the single-objective, indicating the improved process representation of the
377 behavior parameters by the triple-objective calibration. Through 150 runs of calibration program, triple-
378 objective calibration got the smallest behavior parameter sets, indicating that involving additional
379 calibration objectives increase the identifiability of model parameters and reduce the equifinality.

380

[Table 3]

381 Fig. 2 shows the uncertainty ranges of the simulations for the behavioral parameters obtained by
382 the three calibration variants. The three variants generally produced similar hydrographs in terms of the
383 magnitudes and timing of peak flows with averaged behavioral parameter sets, but the triple-objective
384 had a narrower uncertainty range, especially for the baseflow dominated periods (Figs. 2a-c). The single-
385 objective variant resulted in rather large uncertainty ranges for the simulations of SCA and isotopic
386 composition (Figs. 2d and g). The good fitness between the simulated and observed streamflow in
387 summer is likely due to the largely overestimated rainfall-triggered surface runoff, because of the
388 underestimated reduction of SCA in spring. The dual-objective calibration significantly reduced the
389 uncertainty range of the SCA simulation, and captured the declining SCA in summer very well (Fig. 2e).
390 Including SCA in the model calibration, however, only provided small benefits for the simulation of $\delta^{18}\text{O}$
391 in stream water (Fig. 2h). Simulations of the triple-objective variant properly reproduced the temporal
392 variation in SCA in the melt season, despite the slightly reduced performance compared to that of the
393 dual-objective variant (behaving as higher MAE_{SCA} of triple-objective calibration in Table 3). Meanwhile,
394 the seasonal variations of $\delta^{18}\text{O}$ of stream water were reproduced well by the triple-objective calibration
395 (Fig. 2i).

396

[Figure 2]

397 Fig. 3a shows median value of the simulated daily inputs of water sources (rainfall, snowmelt, and
398 glacier melt) for the calibration period obtained by the behavioral parameter sets of the triple-objective
399 variant. All the three water sources started to contribute to stream water in around April. The volume of
400 snowmelt peaked around June, and then decreased rapidly in July as the catchment SCA decreased
401 significantly. The volumes of rainfall and glacier melt peaked in mid-summer which was the wettest and

402 warmest period in the year. The fluctuations of the simulated $\delta^{18}\text{O}$ of stream water in Fig. 3b are generally
403 consistent with the varying contributions of these water sources to runoff. At the beginning of the wet
404 season, $\delta^{18}\text{O}$ of stream water increased rapidly in response to the dominance of the isotopic enriched
405 precipitation. The $\delta^{18}\text{O}$ of stream water began to decrease in the late wet season, likely because of the
406 reduced $\delta^{18}\text{O}$ of precipitation caused by the reported as “temperature effect” (Dansgaard, 1964) and which
407 wasis mainly due to the effect of southwest monsoon (Yin et al., 2006), as well as the increased
408 contributions of isotopic depleted glacier melt.

409

[Figure 3]

410 3.2 Contributions of runoff components

411 The results of runoff component quantification reported in this section were based on the behavioral
412 parameter sets of the three calibration variants. Table 4 and Figure 4 shows the proportions of water
413 sources in the mean annual water input during 1st January 2007 to 31st December 2011. In all the three
414 calibration variants rainfall provided most of the water quantity for runoff generation (44.2% to 48.0%),
415 because of the high partition of rainfall (around 347mm) in the annual precipitation (around 587mm).
416 The single-objective variant estimated the lowest proportion of snowmelt (19.7%), because the
417 simulation of SCA was not constrained in the calibration, leading to largely overestimated SCA in
418 comparison to the MODIS SCA estimates due to less melting (Fig. 2d). The dual-objective variant
419 estimated the highest proportion of glacier melt (33.8%), resulting in a lower proportion of rainfall
420 (44.2%). Involving the calibration objective of isotope, the triple-objective variant estimated the lowest
421 proportion of glacier melt (29.2%) by rejecting the parameter sets that produced high contribution of
422 glacier melt (as shown in Fig. 4), which will be discussed more in detailed in the discussion section. To
423 be noted, despite above differences, the results of three calibration variant were quite similar, with the
424 maximum difference lower than 5%. However, the uncertainties of the simulated water proportions
425 decreased substantially with the increase of data that was involved in the calibration, showing as a
426 decreasing uncertainty (12.4% to 6.2%, Table 4) and fewer outliers (Fig. 4), demonstrating considerable
427 values of additional datasets for constraining the simulations of corresponding runoff generation
428 processes.

429

[Table 4 Table-4]

430

[Figure 4]

431 Fig. 5 and Table 4 compares the seasonal proportions of water sources in the total water input of the
432 three calibration variants. The seasonal dominance of the water sources on runoff estimated by the three
433 calibration variants are similar. In particular, the proportion of rainfall was large (around 55%) in summer
434 but small in winter when rainfall rarely occurred. Snowmelt and glacier melt dominated the total water
435 input in winter with proportions of around 60% and 40%, respectively. The proportion of meltwater in
436 summer was relatively low because of the dominance of rainfall during the summer monsoon. Snowmelt
437 could only account for around 15% in the total water input in summer because of the significantly reduced
438 snowpack. The proportion of glacier melt was higher than that of snowmelt in summer because of the
439 decreasing snow cover area. In the spring months, snowmelt and glacier melt contributed around 55%-
440 60% and 35%-30% to the total water input, respectively, and r- Rainfall provided the remaining 5%. The
441 glacier melt provided a steady contribution of around 30%-40% throughout the entire hydrological year.
442 The seasonal proportions of water sources show slightly different among the calibration variants.
443 Specifically, the triple-objective calibration estimated not only the highest snowmelt and lowest glacier

444 melt in the three seasons except winter, but also the highest contribution of rainfall in summer (Fig. 5c),
445 which was consistent with the lowest contribution of glacier melt in total water input estimated by triple-
446 objective calibration. Single-objective calibration produced the highest contribution of rainfall in autumn,
447 and the highest contribution of snowmelt in winter (Fig. 5a). Although the contribution of water sources
448 had exhibited a large uncertainty in winter, and significant difference existed among the calibration
449 variants, it had negligible effect on the annual result, because of the extremely low contribution of water
450 input during winter (<1%). In addition, The uncertainty ranges of the seasonal proportion during summer
451 and autumn were obviously reduced by the triple-objective calibration (Fig. 5c).

452 [Figure 5]

453 Table 5 shows the contributions of runoff components to annual and seasonal runoff. Three
454 calibration variants resulted in rather similar contributions of surface runoff and subsurface runoff
455 (around 65% and 35% respectively). Surface runoff was the dominant component in this catchment,
456 because of the large glacier covered area (around 20%) and the large saturation area (around 20%). The
457 triple-objective calibration estimated relatively lowest surface runoff (64.9%) and highest subsurface
458 runoff (35.1%). Surface runoff dominated the runoffstreamflow during spring and summer (with
459 proportions of around 65% and 80%, respectively), when large rainfall and snowmelt events occurred
460 frequently and the catchment was rather wet. Subsurface runoff played a more important role during
461 autumn, accounting for about 60% of the runoff. The runoff in winter was dominated by baseflow,
462 because of the very rare water input events. Again, the triple-objective calibration resulted in lowest
463 uncertainty ranges for the contributions of the runoff components compared to the other two calibration
464 variants (4.1% compared to 12.1%). Isotope data used in the triple-objective variant provided additional
465 constraints on the estimation of parameters controlling the generation of subsurface flow (such as *KKA*
466 and *KKD* in Table 2) and the saturation area where surface runoff occurred (such as *WM* and *B*), thus
467 constraining the partitioning between surface runoff and subsurface runoff.

468 [Table 5]

469 3.3 Estimations of water travel time and residence time

470 The travel time and residence time were estimated for the five water years (2007/1/1 – 2011/12/31)
471 during the simulation period. The result produced by the best parameter set (($NSE_{dis} = 0.72$, $MAE_{SCA} =$
472 0.079 , $MAE_{iso} = 0.484$) was used to test the consistency between the two model-based methods. Based
473 on the assumption that glacier melt water had an age of 1000 days, the backward MTT and MRT
474 estimated by MM (FT) method were 1.70 (1.72) and 1.22 (1.17) years, respectively. Fig. 6 shows the
475 comparison between the results of MM and FT methods. As shown in Fig. 6a and 6d, there were strong
476 correlation between the daily MTTs (MRTs) estimated by the two methods with a high correlation
477 coefficient of 0.96 (0.98). The daily MTT and MRT series also showed similar temporal variability
478 between the two methods as shown in Fig. 6b and 6e. The MRT increased steadily during dry season,
479 and decreased rapidly during wet season due to the recharge of young precipitation. The daily MTT also
480 showed steady increasing trend during dry season, but showed significant fluctuation during wet season
481 because of the combined effect of young precipitation and old glacier meltwater. Fig. 6c and 6e shows
482 the probability density function of the daily backward MTT and MRT produced by the two methods. The
483 daily MTT had a large range from 0.42 to 2.75 years, with several peak density values at around 1, 1.5
484 and 2.67 years, including the influence of the multiple water sources with different ages. On the contrary,
485 the daily MRT only had a narrow range from 0.75 to 1.75 years, with a significant peak value at around

486 1.25 years, similar with the MRT. Excluding the effect of glacier meltwater, FT method estimated the
487 precipitation-triggered backward MTT of runoff as 263 days, significantly smaller than the MRT,
488 indicating the incomplete mixing in the catchment scale caused by the distributed modelling framework.

489 **[Figure 6]**

490 The lumped SW method estimated the MTT and MRT as 1.68 years (A_r and A_p were estimated as
491 0.58 and 6.19, respectively). Based on the average result of 19 behavioral parameter sets, the model-
492 based methods estimated the MTT and MRT as 1.61 and 1.28 respectively. The two kinds of methods
493 produced similar MTT, indicating the robustness of travel time estimation in this catchment. The
494 precipitation-triggered MTT (shorter than 1 year) was significantly smaller than the MTT of total runoff
495 estimated by the lumped method, indicating the effect of old glacier melt water. The glacier melt
496 contributed to stream water through surface runoff directly, and had no contribution to the water storage,
497 leading to a smaller model-based MRT compared to MTT. The uncertainty of MTT and MRT estimation
498 could be reflected by the range produced by MM method by the 19 behavioral parameter sets as shown
499 in Fig. 7. The standard deviation of the estimated MTT and MRT were 74 and 79 days, respectively. The
500 uncertainty range during June to August was relatively small (Fig. 7a), indicating that different behavioral
501 parameters produced similar precipitation-triggered processes during the wet season, and the uncertainty
502 mainly came from the large range of MRT, i.e., the age of water storage including soil water and
503 groundwater.

504 **[Figure 7]**

505 Based on the best parameter set, FT method tracked the transportation of precipitation and produced
506 time-varying forward TTD, backward TTD and RTD. For simplicity, Fig. 8 shows the average
507 distributions weighted by the precipitation amount (for forward TTD), runoff generation (for backward
508 TTD) and water storage (for RTD). As shown in Fig. 8a and 8b, the forward and backward TTD were
509 similar, behaving as a high proportion (~0.3) of the youngest water, which was consistent with the high
510 proportion of rapid surface runoff. The high proportion of young water led to a similar TTD form as
511 exponential model. The relative peaks of TTD were mainly around the travel time of integral years,
512 indicating the influence of baseflow from groundwater, which were recharged by precipitation in the wet
513 seasons of previous years. The simulated RTD was significantly different from the TTD, behaving as the
514 low probability density of young water. The young water was mainly recharged by the infiltrating rainfall
515 and snowmelt, which was negligible compared to the total water storage. Again, the difference between
516 TTD and RTD indicated the incomplete mixing processes, behaving as affinity for young water due to
517 the rapid flow pathways such as surface runoff.

518 **[Figure 8]**

519 **4. Discussions**

520 **4.1 The values of tracer on constraining flow pathways and water storages in the hydrological** 521 **model**

522 This study developed a tracer-aided hydrological model and tested its behavior in a glacierized
523 catchment. Because of the sampling difficulties on the Tibetan Plateau, the tracer data of the water
524 sources (e.g., snow, glacier, groundwater) was rather limited compared to other tracer-aided modelling
525 works (e.g., Ala-aho et al., 2017; He et al., 2019). Nonetheless, the model developed in this study
526 performed well on producing the tracer signature of stream water, producing a tool for applying the

527 tracer-aided method to the areas with limited tracer data. Although it was widely accepted that simple
528 input-output tracer measurements provided limited insight into catchment function, and sampling source
529 water components would be helpful (Birkel et al., 2014; Tetzlaff et al., 2014), the uncertainty of model
530 could still be reduced significantly by satisfying the output tracer signature (Delavau et al., 2017),
531 especially in cold regions where hydrological processes were more complex. The fact that the model can
532 simultaneously satisfy three calibration objectives over a long period gave confidence in the model
533 realizations (McDonnell and Beven, 2014).

534 Our results indicate that involving the isotope into calibration significantly reduced the uncertainty
535 of quantifying the runoff components. To understand the role of isotope data on reducing the uncertainty,
536 the results of dual-objective calibration variant were analyzed why some of the parameter sets behaved
537 poorly on isotope simulation despite their good performance on discharge and snow simulation. Among
538 the 117 behavioral parameter sets of dual-objective calibration, only 14 of them produced relatively good
539 isotope simulations ($MAE_{iso} < 1.0$). As shown in Fig. 9a and 9b, these 14 isotopic behavioral parameter
540 sets produced the proportion of runoff component within a relatively smaller range (27.5% to 38% for
541 glacier melt, and 58% to 75% for surface runoff), while the 117 behavioral parameter sets produced a
542 much larger variation (24% to 53% for glacier melt, and 40% to 90% for surface runoff). This indicated
543 that involving isotope data for model calibration helped to exclude some unreasonable proportions of
544 runoff component. The distribution of scatter in Fig. 9a and Fig. 9b was similar, and the proportion of
545 surface runoff had a strong correlation with the proportion of glacier melt as shown in Fig. 9c (because
546 of the assumption that glacier melt contributed to surface runoff directly), thus the mechanism that
547 isotope can reject unreasonable proportions were the same for water sources and runoff generation
548 processes. Fig. 9d shows the simulation range of $\delta^{18}O$ of stream water by calibrated parameters that
549 resulted in glacier melt proportion in the total water input higher than 40%. The simulated isotopic
550 signature showed strong fluctuations due to the high proportion of surface runoff with a larger time
551 variation compared to the relatively steady signature of subsurface runoff. Also, the simulated isotopic
552 values were significantly higher than the observations, which was mainly the result of the excessive
553 isotopic fractionation due to the too much evaporation of surface water (Hindshaw et al., 2011; Wolfe et
554 al., 2007). Fig. 9e shows the simulation range by the parameters with proportion of surface runoff lower
555 than 45%. In contrast to scenarios with too high glacier melt, the simulated isotope signature showed
556 small variation and the mean values were much lower than the observation. Our result also showed that
557 the proportion of surface runoff and glacier melt tended to be higher when the NSE_{dis} was higher,
558 indicating that focusing on the simulation of integrated observation of discharge only will likely lead to
559 overestimated surface runoff and glacier melt. These results indicated that the isotope data helped to
560 constrain the quantifications of runoff components by (1) regulating the competition between rapid
561 component with strong variation of isotope signatures (e.g., surface runoff) and slow component with
562 relatively stable isotope signatures (e.g., subsurface runoff) to match the daily fluctuations of observed
563 isotope signature of stream water, and (2) controlling the isotopic fractionation by adjusting the
564 evaporation to satisfy the observed isotopic value.

565 **[Figure 9]**

566 Two model-based methods (MM and FT) were adopted to estimate travel time and residence time
567 in this study, and verified by the result of lumped method (SW). Both MM and FT methods can estimate
568 MTT and MRT, but FT provided more information including TTD and RTD, which was actually more
569 of interest. MM method has been used in several previous studies, including modelling work in snow-

570 influenced basins (Ala-aho et al., 2017). Consequently, the results of FT and MM were compared in this
571 study, to ensure that the additional information provided by FT method was reasonable. Our result
572 indicated that the two model-based methods produced consistent results, which were also similar with
573 the lumped method, indicating the robustness of MTT and MRT estimation through a tracer-aided model
574 without defining any prior distribution functions.

575 Although significantly constraining the proportion of runoff component, the uncertainty ranges of
576 simulated MTT and MRT, especially that during baseflow-dominant period (as shown in Fig. 7b) were
577 still rather large, indicating that the estimation of groundwater age had a large uncertainty, which was
578 similar with other model-based age estimation works (e.g., Ala-aho et al., 2017; van Huijgevoort et al.,
579 2016). The isotope observations were mainly collected during wet season when precipitation-triggered
580 surface runoff played an important role in runoff generation, thus this process was constrained relatively
581 well by the isotope calibration, showing as the similar fluctuation of MTT during wet season produced
582 by different parameter sets. Although the proportion of subsurface runoff was constrained, the storage
583 volume of groundwater was poorly constrained, because of the relatively simplified structure of the
584 groundwater module of THREW model (Tian et al., 2006), which adopted a two-layer reservoir model
585 to describe the processes of seepage and subsurface flow. Apart from involving more calibration
586 objectives, improving the physical mechanism and the representation of hydrological processes is another
587 important way to constrain the model behavior and reduce uncertainties.

588 4.2 Insight from MTT and MRT estimation

589 Based on three MTT estimation methods, this study estimated the MTT and MRT as 1.7 and 1.2
590 years, reflecting the age of stream water and subsurface water storage in the catchment. Excluding the
591 effect of ~~old~~aged glacier meltwater, the MTT of stream water fed by rainfall and snowmelt decreased to
592 around 9 months. Ala-aho et al. (2017) estimated the median water ages of three snow influenced
593 catchments located in the USA, Sweden and Scotland using the MM method as 11 months, 1.5 years and
594 5 years. The water age had a rather wide range among different catchments, which mainly dependeds on
595 the groundwater storage controlled by the topography and soil characteristics. The process that water
596 travel through the subsurface pathway play comparable role with the snow accumulation process on the
597 water age in snow influenced catchment. The significantly lower MTT and MRT estimated in this study
598 than that of the three catchments in Ala-aho et al. (2017) ~~was~~can be mainly ~~due~~attributed to the large
599 impermeable area on the glacier, leading to a large proportion of surface runoff with very short travel
600 time.

601 The influence factors of the MTT and MRT were analyzed to better understand the hydrological
602 processes in the catchment. The relationship between the daily travel times (including forward MTT,
603 backward MTT and MRT) and the environmental factors (including simulated soil water content and
604 meteorological factors) was analyzed in- Fig. 10. The result shows the scatter diagrams between the
605 factors with good correlation. MRT ~~had~~presented a strong negative correlation with the soil water content
606 (Fig. 10a), which was consistent with the finding by Hrachowitz et al. (2013) and Heidebuechel et al.
607 (2012) that the resident water age was sensitive to antecedent wetness and the water stored in subsurface
608 storage. During dry season, the MRT got older as time went on, and the soil water content was decreasing
609 due to the outflow of groundwater. The soil water content increased rapidly during wet season when
610 precipitation occurred and recharged the groundwater, and the MRT got younger due to the recharge of
611 young water. Backward MTT had good relationship with both soil water (Fig. 10b) and precipitation

612 amount (Fig. 10c). During dry season when runoff was mainly baseflow, the age of stream water was
613 similar with the groundwater and consequently controlled by the soil water content. During wet season,
614 the backward MTT was largely dependent on the precipitation amount, because a large proportion of
615 young precipitation event water contributed to stream water quickly through surface runoff pathway,
616 leading to small MTT. This was also consistent with the result reported by Hrachowitz et al. (2013) and
617 McMillan et al. (2012) that the water flux age was controlled by fast and slow processes under wetting-
618 up and drying-up conditions. The forward MTT reflected the time that the input water took to travel
619 through the catchment, showing good relationship with temperature (Fig. 10d). The negative correlation
620 between forward MTT and temperature was mainly related to two processes, i.e., the snow accumulation,
621 and the evaporation. When the temperature was low, the precipitation was mainly in the form of snowfall,
622 which cannot contribute to the stream quickly, resulting in a long travel time. On the contrary, the water
623 would be exposed to intense evaporation when the temperature was high. Large proportion of
624 precipitation event water left the catchment quickly by evaporation before infiltrating into groundwater
625 and going through the long subsurface pathway, resulting in a short travel time. The negative relation
626 between forward MTT and temperature indicated an accelerated water cycling process as a result of
627 climate warming.

628 **[Figure 10]**

629 **4.3.2 Limitation and uncertainty**

630 Multiple water sources brought difficulties to hydrological modelling in glacierized basins
631 (Zongxing et al., 2019). Focusing on the tracer transportation processes, the model developed in this
632 study made some simplifications on the processes related to snow and glacier to make the model structure
633 parsimonious. First, the snow accumulation and melting processes were simulated by a simple
634 temperature-based method, which was relatively lack of physical mechanism compared to the energy-
635 based methods (e.g., Pomeroy et al., 2007). Nonetheless, this method had an acceptable behavior and
636 was widely used in studies of snow simulation (e.g., He et al., 2014), and the simulated SCA was
637 validated by the MODIS data during ablation period in this study. Second, the evolutions of glacier
638 thickness and area were not simulated in the model. Simplification of a constant glacier area likely led
639 to an overestimation of the contribution of glacier melt to runoff, as the glacier cover area should get
640 smaller due to the climate warming. However, this simplification should have minor influence on the
641 result because the changes of glacier area was rather small in a short simulation period of seven years.

642 The influence of calibration objective function was inadequately assessed in this study. Although
643 the measurement units of NSE_{dis} was different from the MAE_{SCA} and MAE_{iso} , their values were in the
644 same order of magnitude when the model performance were acceptable (similarly with He et al., 2019).
645 Consequently, they were combined directly to reflect the simultaneous performance on the three
646 objectives. Plenty of studies have developed methods to solve the problem of multiple objective
647 calibration by introducing an integrated evaluation metric (e.g., Gupta et al., 2009; Shafii and Tolson,
648 2015) or giving weights to each objective (e.g., Tong et al., 2021). This study mainly aimed to evaluate
649 the value of isotope data on improving the model behavior, rather than developing a general calibration
650 strategy, thus the three evaluation metrics were added together with equal weights for simplification, to
651 represent the condition that all the three objectives were simulated well. Our main findings indicated that
652 the results calibrated by discharge and isotope were more behavioral in many aspects than the results
653 calibrated only by discharge. The potential influences of calibration metrics and methods on the finally

654 [optimized result still needed further exploration.](#)

655 _____The lack of source water sampling made it difficult to fully validate the modelling result.
656 Although the isotope signature of stream water was reproduced well, it cannot guarantee that the isotopic
657 variations of groundwater, snowmelt were simulated correctly. The quantification of runoff components
658 was also hard to verified. The end-member method cannot be applied as a reference due to the lack of
659 water source tracer data. A previous study of snow cover and runoff modelling work in the same basin
660 (Zhang et al., 2015) provided a potential reference. That work indicated that the contribution of rainfall,
661 snowmelt and glacier melt in 2006 were 30%, 10% and 60%, respectively, which was markedly different
662 from the result of this study. The runoff simulation in Zhang et al. (2015) was conducted by a simplified
663 conceptual model with limited physical mechanism, which did not consider the processes of subsurface
664 runoff and evaporation. And the glacier melt runoff coefficient (the ratio of glacier melt runoff to the total
665 glacier melt) estimated by that study was very small (0.182), indicating that a large proportion of glacier
666 melt did not contribute to the surface runoff directly, which is inconsistent with the common assumption
667 in previous studies (e.g., Seibert et al., 2018; Schaefer et al., 2005). The extremely low glacier melt runoff
668 coefficient might lead to overestimation of the contribution of glacier melt. The significant differences
669 between the two studies mainly resulted from the difference of model structure. Intensive source water
670 sampling together with systematic glacier observation might improve the behavior of hydrological model
671 in glacierized basins and help us better understand the runoff processes.

672 In glacierized basins where glacier meltwater played an important role on runoff generation, the
673 object of the three MTT estimation methods were different. The total runoff could be divided into
674 precipitation-triggered runoff (including rainfall-runoff and snowfall-snowmelt-runoff) and glacier melt
675 runoff. Considering that glacier was also formed by the precipitation over past years, the lumped SW
676 method should have reflected both runoff processes, because it was based on the tracer data of
677 precipitation and total runoff. The two model-based methods mainly focused on the precipitation-
678 triggered runoff, because the glacier revolution process was simplified in the model. The MTT estimation
679 of total runoff should be based on the assumed MTT of glacier melt water. In this study, assuming the
680 MTT of glacier melt as 1000 days, the model-based results were similar with SW method, indicating that
681 the assumption of glacier melt MTT was appropriate, which was actually misleading. The time scale of
682 glacier update was much longer than this assumed value, because glacier generally took decades to
683 hundreds of years to move from accumulation zone to ablation zone (Soncini et al., 2014; Yao et al.,
684 2012). The good agreement among the three methods indicate that the SW method significantly
685 underestimated the age of glacier. This was mainly due to the limited applicable time scale of stable
686 isotope in water. It was reported that seasonal cycle of stable isotope in precipitation were most useful
687 for inferring relatively short travel time of 2-4 years (McGuire and McDonnell, 2006; Sprenger et al.,
688 2019; Stewart et al., 2010). The assumed glacier melt MTT of 1000 days was within this range, thus the
689 similar result of three methods could verify the model representation of the precipitation-triggered runoff
690 process, and the cross validation between MM and FT methods further enhanced the robustness of the
691 travel time estimation. Consequently, we can expect that if a tracer suitable for longer travel time (e.g.,
692 ^{14}C) was used to estimate the proper MTT of total runoff, we could better infer the age of water according
693 to the model-based estimation of precipitation-triggered runoff MTT.

694 **5. Conclusions**

695 A tracer module was integrated into the THREW hydrological model to constrain the various runoff

696 processes, and was tested in a glacierized catchment on the Tibetan Plateau. Measurements of oxygen
697 stable isotopes of the stream water were used to calibrate the model parameters, in addition to the
698 observations of discharge and MODIS SCA. The behaviors of the model, especially the quantifications
699 of runoff components were compared among the calibration variants with different objective, to test the
700 value of isotope data on constraining the model parameters. A lumped method (SW) and two model-
701 based methods (MM and FT) were applied to estimate the water travel time in the study basin. Our main
702 findings are: _

703 (1) The THREW-t model performed well on simultaneously reproducing the variations of discharge,
704 snow cover area, and the isotopic composition of stream water, despite of a small water sample number
705 of precipitation was available to provide isotope input data.

706 (2) The contributions of rainfall, snowmelt and glacier melt to the annual runoff were quantified as
707 47.4%, 23.4% and 29.2%. Surface runoff (contributing around 64.9%) was more dominant than
708 subsurface flow in the annual runoff. Calibration with isotope data significantly reduced the uncertainties
709 by regulating the competition between rapid and slow runoff components to fit the variation of observed
710 isotope signature, and resulted in more plausible quantifications of contributions of runoff components
711 to seasonal runoff. _

712 (3) The estimated MTT of model-based methods MM and FT met well with that of a sin-wave
713 lumped parameter method, indicating the robustness of travel time estimation benefiting from the use of
714 water isotope data. The precipitation-triggered MTT was significantly shorter than the MTT of total
715 runoff, indicating the effect of old glacier meltwater. The MRT was longer than precipitation-triggered
716 MTT, indicating the catchment scale incomplete mixing processes, and the affinity for young water due
717 to the rapid flow pathways such as runoff on impermeable glacier surface. The temporal variation of
718 MTT and MRT was dependent on the catchment wetness conditions and meteorological factors.

719 **Code/Data availability**

720 The isotope data and the code of THREW-t model used in this study are available by contacting the
721 authors.

722 **Author contribution**

723 YN, ZH and FT conceived the idea; LT provided the observation data; YN, FT, LT and ZH conducted
724 analysis; LS provided comments on the analysis; all the authors contributed to writing and revisions.

725 **Competing interests**

726 The authors declare that they have no conflict of interest.

727 **Acknowledgements**

728 This study was supported by the National Science Foundation of China (92047301, 91647205). The
729 authors would like to thank Kunbiao Li from Tsinghua University for the contribution of the coding of
730 calibration program. The authors thank all the organizations and scientists for the contribution of data
731 used in this work. Datasets of glacier, snow cover and vegetation for this study are available in these in-
732 text data citation referees: Liu (2012), Hall and Riggs (2016), Didan (2015) and Myneni et al. (2015).
733 The digital elevation model (DEM) data set is available at Geospatial Data Cloud site, Computer Network
734 Information Center, Chinese Academy of Sciences (<http://www.gscloud.cn>). The meteorological data is

735 available at China Meteorological Data System (<http://data.cma.cn>). The soil data is available at the Food
736 and Agriculture Organization of the United Nations (<http://www.fao.org/geonetwork/>). All the data used
737 in this study will be available at the Zenodo website at the time of publication or on request from the
738 corresponding author (tianfq@mail.tsinghua.edu.cn).

739 **Financial support**

740 This study was supported by the National Science Foundation of China (grant no. 92047301, 91647205).

741 **References**

742 Ala-Aho, P. , Tetzlaff, D. , Mcnamara, J. P. , Laudon, H. , & Soulsby, C. . (2017). Using isotopes to
743 constrain water flux and age estimates in snow-influenced catchments using the starr (spatially
744 distributed tracer-aided rainfall–runoff) model. *Hydrology and Earth System Sciences*
745 *Discussions*, 21(10), 5089-5110.

746 Benettin, P., & Bertuzzo, E. (2018). tran-SAS v1. 0: a numerical model to compute catchment-scale
747 hydrologic transport using StorAge Selection functions. *Geoscientific Model Development*, 11(4),
748 1627-1639.

749 Birkel, C. , Soulsby, C. , & Tetzlaff, D. . (2014). Developing a consistent process-based conceptualization
750 of catchment functioning using measurements of internal state variables. *Water Resources Research*,
751 50(4), 3481–3501.

752 Birkel, C., Tetzlaff, D., Dunn, S. M., & Soulsby, C. (2011). Using time domain and geographic source
753 tracers to conceptualize streamflow generation processes in lumped rainfall-runoff models. *Water*
754 *Resources Research*, 47(2).

755 Botter, G. , Bertuzzo, E. , & Rinaldo, A. . (2011). Catchment residence and travel time distributions: the
756 master equation. *Geophysical Research Letters*, 38(11).

757 [Bowen, G. J., Cai, Z., Fiorella, R. P., & Putman, A. L. \(2019\). Isotopes in the water cycle: regional-to](#)
758 [global-scale patterns and applications. *Annual Review of Earth and Planetary Sciences*, 47, 453-479.](#)

759 Capell, R., Tetzlaff, D., & Soulsby, C. (2012). Can time domain and source area tracers reduce uncertainty
760 in rainfall-runoff models in larger heterogeneous catchments?. *Water Resources Research*, 48(9).

761 Chen, X. , Long, D. , Hong, Y. , Zeng, C. , & Yan, D. . (2017). Improved modeling of snow and glacier
762 melting by a progressive two-stage calibration strategy with grace and multisource data: how snow
763 and glacier meltwater contributes to the runoff of the upper brahmaputra river basin?. *Water resources*
764 *research*, 53(3), 2431-2466.

765 Dansgaard, W. (1964). Stable isotopes in precipitation. *Tellus*, 16(4), 436-468.

766 Delavau, C. J., Stadnyk, T., & Holmes, T. (2017). Examining the impacts of precipitation isotope input
767 ($\delta^{18}\text{O}_{\text{ppt}}$) on distributed, tracer-aided hydrological modelling. *Hydrology and Earth System*
768 *Sciences*, 21(5), 2595-2614.

769 Didan, K. (2015). MOD13A3 MODIS/Terra vegetation Indices Monthly L3 Global 1km SIN Grid V006
770 [Data set]. NASA EOSDIS Land Processes DAAC. Accessed 2020-01-01 from
771 <https://doi.org/10.5067/MODIS/MOD13A3.006>

772 Dou, Y. , Chen, X. , Bao, A. , & Li, L. . (2011). The simulation of snowmelt runoff in the ungauged kaidu
773 river basin of tianshan mountains, china. *Environmental Earth Sciences*, 62(5), 1039-1045.

774 Duethmann, D., Bolch, T., Farinotti, D., Kriegel, D., Vorogushyn, S., Merz, B., ... & Güntner, A. (2015).
775 Attribution of streamflow trends in snow and glacier melt-dominated catchments of the T arim R iver,
776 Central A sia. *Water Resources Research*, 51(6), 4727-4750.

777 Duethmann, D., Peters, J., Blume, T., Vorogushyn, S., & Güntner, A. (2014). The value of satellite-
778 derived snow cover images for calibrating a hydrological model in snow-dominated catchments in
779 Central Asia. *Water resources research*, 50(3), 2002-2021.

780 Eriksson, D., Bindel, D., & Shoemaker, C. (2015). Surrogate optimization toolbox (pysot).

781 Finger, D. , Vis, M. , Huss, M. , & Seibert, J. . (2015). The value of multiple data set calibration versus
782 model complexity for improving the performance of hydrological models in mountain
783 catchments. *Water resources research*, 51(4), 1939-1958.

784 Gao J. , Tian L. , & Liu Y. (2009). Oxygen isotope variation in the water cycle of the Yamdrok-tso Lake
785 Basin in southern Tibetan Plateau. *Chinese Sci Bull*, 54: 2758—2765

786 [Gupta, H. V. , Kling, H. , Yilmaz, K. K. , & Martinez, G. F. . \(2009\). Decomposition of the mean squared
787 error and nse performance criteria: implications for improving hydrological modelling. *Journal of
788 Hydrology*, 377\(1\), 80-91.](#)

789 Garvelmann, Jakob, Warscher, Michael, Leonhardt, Gabriele, Franz, Helmut, Lotz, Annette, &
790 Kunstmann, Harald. (2017). Quantification and characterization of the dynamics of spring and stream
791 water systems in the berchtesgaden alps with a long-term stable isotope dataset. *Environmental Earth
792 Sciences*, 76(22), 766.

793 [Gat, J. R. \(1996\). Oxygen and hydrogen isotopes in the hydrologic cycle. *Annual Review of Earth and
794 Planetary Sciences*, 24\(1\), 225-262.](#)

795 Hall, D. K. and G. A. Riggs. (2016). MODIS/Terra Snow Cover 8-Day L3 Global 500m SIN Grid,
796 Version 6. [Data set]. Boulder, Colorado USA. NASA National Snow and Ice Data Center Distributed
797 Active Archive Center. Accessed 2020-01-01 from <https://doi.org/10.5067/MODIS/MOD10A2.006>.

798 Harman, C. J. . (2019). Age - ranked storage - discharge relations: a unified description of spatially
799 lumped flow and water age in hydrologic systems. *Water Resources Research*, 55(8).

800 He, Z. H., Parajka, J., Tian, F. Q., & Blöschl, G. (2014). Estimating degree day factors from MODIS for
801 snowmelt runoff modeling. *Hydrology & Earth System Sciences Discussions*, 11(7).

802 He, Z. H., Tian, F. Q., Gupta, H. V., Hu, H. C., & Hu, H. P. (2015). Diagnostic calibration of a hydrological

803 model in a mountain area by hydrograph partitioning. *Hydrology and Earth System Sciences*, 19(4),
804 1807.

805 He, Z. , Vorogushyn, S. , Unger-Shayesteh, K. , Gafurov, A. , Kalashnikova, O. , & Omorova, E. , et al.
806 (2018). The value of hydrograph partitioning curves for calibrating hydrological models in glacierized
807 basins. *Water Resources Research*, 54(3), 2336-2361.

808 He, Z. , Unger-Shayesteh, K. , Vorogushyn, S. , Weise, S. M. , Kalashnikova, O. , & Gafurov, A. , et al.
809 (2019). Constraining hydrological model parameters using water isotopic compositions in a
810 glacierized basin, central asia. *Journal of Hydrology*.

811 He, Z., Unger-Shayesteh, K., Vorogushyn, S., Weise, S., Duethmann, D., Kalashnikova, O., Gafurov, A.,
812 Merz, B., 2020. Comparing Bayesian and traditional end-member mixing approaches for hydrograph
813 separation in a glacierized basin. *Hydrol. Earth Syst. Sci. Hydrol. Earth Syst. Sci.*, 24, 3289–3309,
814 <https://doi.org/10.5194/hess-24-3289-2020>

815 Heidbuechel, I. , Troch, P. A. , Lyon, S. W. , & Weiler, M. . (2012). The master transit time
816 distribution of variable flow systems. *Water Resources Research*, 48(6), 6520.

817 Hindshaw, R. S., Tipper, E. T., Reynolds, B. C., Lemarchand, E., Wiederhold, J. G., Magnusson, J., ... &
818 Bourdon, B. (2011). Hydrological control of stream water chemistry in a glacial catchment (Damma
819 Glacier, Switzerland). *Chemical Geology*, 285(1-4), 215-230.

820 Hrachowitz, M. , Savenije, H. , Bogaard, T. A. , Tetzlaff, D. , & Soulsby, C. . (2013). What can flux
821 tracking teach us about water age distribution patterns and their temporal dynamics?. *Hydrology and*
822 *Earth System Sciences*, 17(2), 533-564.

823 Immerzeel, W.W., Pellicciotti, F., Bierkens, M.F.P., 2013. Rising river flows throughout the twenty-first
824 century in two Himalayan glacierized watersheds. *Nat. Geosci.* 6, 742–745.
825 <https://doi.org/10.1038/ngeo1896>

826 Immerzeel, W. W., Van Beek, L. P., & Bierkens, M. F. (2010). Climate change will affect the Asian water
827 towers. *Science*, 328(5984), 1382-1385.

828 Kirchner, J. W. (2016). Aggregation in environmental systems - part 1: seasonal tracer cycles quantify
829 young water fractions, but not mean transit times, in spatially heterogeneous catchments. *Hydrology*
830 *& Earth System Sciences*.

831 Kong, Y., Pang, Z., 2012. Evaluating the sensitivity of glacier rivers to climate change based on
832 hydrograph separation of discharge. *J. Hydrol.* 434–435, 121–129.
833 <https://doi.org/10.1016/j.jhydrol.2012.02.029>

834 Kong, Y., Wang, K., Pu, T., & Shi, X. (2019). Nonmonsoon precipitation dominates groundwater recharge
835 beneath a monsoon - affected glacier in Tibetan Plateau. *Journal of Geophysical Research:*
836 *Atmospheres*, 124(20), 10913-10930.

837 Konz, M., & Seibert, J. (2010). On the value of glacier mass balances for hydrological model

838 calibration. *Journal of hydrology*, 385(1-4), 238-246.

839 Kumar, R. , Singh, S. , Kumar, R. , Singh, A. , Bhardwaj, A. , & Sam, L. , et al. (2016). Development of
840 a glacio-hydrological model for discharge and mass balance reconstruction. *Water Resources*
841 *Management*, 30(10), 3475-3492.

842 Liu, Z., Tian, L., Yao, T., Gong, T., Yin, C., & Yu, W. (2007). Temporal and spatial variations of $\delta^{18}\text{O}$
843 in precipitation of the Yarlung Zangbo River Basin. *Journal of Geographical Sciences*, 17(3), 317-
844 326.

845 Liu S. (2012). The second glacier inventory dataset of China (version 1.0) (2006-2011) [Data set].
846 National Tibetan Plateau Data Center. Accessed 2020-01-01 from
847 <https://doi.org/10.3972/glacier.001.2013.db>.

848 Luo, Y. , Wang, X. , Piao, S. , Sun, L. , Ciais, P. , & Zhang, Y. , et al. (2018). Contrasting streamflow
849 regimes induced by melting glaciers across the tien shan – pamir – north karakoram. *Scientific*
850 *Reports*, 8(1).

851 Lutz, A. F. , Immerzeel, W. W. , Shrestha, A. B. , & Bierkens, M. F. P. . (2014). Consistent increase in
852 high asia's runoff due to increasing glacier melt and precipitation. *Nature Climate Change*.

853 Lutz, A.F., Immerzeel, W.W., Kraaijenbrink, P.D.A., Shrestha, A.B., Bierkens, M.F.P., 2016. Climate
854 Change Impacts on the Upper Indus Hydrology: Sources , Shifts and Extremes 1–33.
855 <https://doi.org/10.1371/journal.pone.0165630>

856 Marques, J. E. , Samper, J. , Pisani, B. , Alvares, D. , Carvalho, J. M. , & H. I. Chaminé, et al. (2011).
857 Evaluation of water resources in a high-mountain basin in serra da estrela, central portugal, using a
858 semi-distributed hydrological model. *Environmental Earth Sciences*, 62(6), 1219-1234.

859 McDonnell, J. J., & Beven, K. (2014). Debates—The future of hydrological sciences: A (common) path
860 forward? A call to action aimed at understanding velocities, celerities and residence time distributions
861 of the headwater hydrograph. *Water Resources Research*, 50(6), 5342-5350.

862 McGuire, K. J. , & McDonnell, J. J. . (2006). A review and evaluation of catchment transit time
863 modeling. *Journal of Hydrology*, 330(3-4), 0-563.

864 McMillan, H., Tetzlaff, D., Clark, M., Soulsby, C., 2012. Do time-variable tracers aid the evaluation of
865 hydrological model structure? A multimodel approach. *Water Resour. Res.* 48.
866 <https://doi.org/10.1029/2011WR011688>

867 Miller, J. D., Immerzeel, W. W., & Rees, G. (2012). Climate change impacts on glacier hydrology and
868 river discharge in the Hindu Kush–Himalayas. *Mountain Research and Development*, 32(4), 461-467.

869 Myneni, R., Knyazikhin, Y., Park, T. (2015). MOD15A2H MODIS/Terra Leaf Area Index/FPAR 8-Day
870 L4 Global 500m SIN Grid V006 [Data set]. NASA EOSDIS Land Processes DAAC. Accessed 2020-
871 01-01 from <https://doi.org/10.5067/MODIS/MOD15A2H.006>

- 872 Mi, D., Xie, Z., & Luo, R. (2001). China Glacier Information System XI: Gangze Water System.
- 873 Nash, J. E., & Sutcliffe, J. V. (1970). River flow forecasting through conceptual models part I—A
874 discussion of principles. *Journal of hydrology*, 10(3), 282-290.
- 875 Nepal, S. , Chen, J. , Penton, D. J. , Neumann, L. E. , Zheng, H. , & Wahid, S. . (2017). Spatial gr4j
876 conceptualization of the tamor glaciated alpine catchment in eastern nepal: evaluation of gr4jsg
877 against streamflow and modis snow extent. *Hydrological Processes*, 31(1), 51-68.
- 878 Nepal, S., Krause, P., Flügel, W., Fink, M., Fischer, C., 2014. Understanding the hydrological system
879 dynamics of a glaciated alpine catchment in the Himalayan region using the J2000 hydrological model.
880 *Hydrol. Process.*, 28, 1329–1344. <https://doi.org/10.1002/hyp.9627>
- 881 Nepal, S., Zheng, H., Penton, D. J., Neumann, L. E., 2015. Comparative performance of GR4JSG and
882 J2000 hydrological models in the Dudh Koshi catchment of the Himalayan region. In MODSIM2015,
883 21st International Congress on Modelling and Simulation, Weber T, McPhee MJ, Anderssen RS (eds).
884 Modelling and Simulation Society of Australia and New Zealand: Gold Coast; 2395–2401. ISBN:978-
885 0-9872143-5-5
- 886 Parajka, J. , & Blöschl, G. . (2008). The value of modis snow cover data in validating and calibrating
887 conceptual hydrologic models. *journal of hydrology*, 358(3-4), 240-258.
- 888 Pomeroy, J. W. , Gray, D. M. , Brown, T. , Hedstrom, N. R. , Quinton, W. L. , & Granger, R. J. , et al.
889 (2007). The cold regions hydrological model: a platform for basing process representation and model
890 structure on physical evidence. *Hydrological Processes*.
- 891 Remondi, F. , Kirchner, J. W. , Burlando, P. , & Fatichi, S. . (2018). Water flux tracking with a distributed
892 hydrological model to quantify controls on the spatiotemporal variability of transit time distributions.
893 *Water Resources Research*, 54(4), 3081-3099.
- 894 Schaefli, B., Hingray, B., Niggli, M., & Musy, A. (2005). A conceptual glacio-hydrological model for
895 high mountainous catchments.
- 896 Schaefli, B., & Huss, M. (2011). Integrating point glacier mass balance observations into hydrologic
897 model identification. *Hydrology and Earth System Sciences*, 15(ARTICLE), 1227-1241.
- 898 Seibert, J. , Vis, M. J. P. , Kohn, I. , Weiler, M. , & Stahl, K. . (2018). Technical note: representing glacier
899 geometry changes in a semi-distributed hydrological model. *Hydrology & Earth System Sciences*
900 *Discussions*, 1-20.
- 901 [Shafii, M. , & Tolson, B. A. . \(2015\). Optimizing hydrological consistency by incorporating hydrological](#)
902 [signatures into model calibration objectives. *Water Resources Research*, 51\(5\), 3796-3814.](#)
- 903 Sivapalan, M. , Takeuchi, K. , Franks, S. W. , Gupta, V. K. , Karambiri, H. , & Lakshmi, V. , et al. (2003).
904 Iahs decade on predictions in ungauged basins (pub), 2003–2012: shaping an exciting future for the
905 hydrological sciences. *International Association of entific Hydrology Bulletin*, 48(6), 857-880.

- 906 Son, K., & Sivapalan, M. (2007). Improving model structure and reducing parameter uncertainty in
907 conceptual water balance models through the use of auxiliary data. *Water resources research*, 43(1).
- 908 Soncini, A., Bocchiola, D., Confortola, G., Bianchi, A., & Diolaiuti, G. (2015). Future hydrological
909 regimes in the upper Indus basin: a case study from a high-altitude glacierized catchment. *Journal of*
910 *Hydrometeorology*, 16(1), 306-326.
- 911 Soulsby, C., Birkel, C., Geris, J., Dick, J., Tunaley, C., Tetzlaff, D., 2015. Stream water age distributions
912 controlled by storage dynamics and nonlinear hydrologic connectivity: Modeling with high-resolution
913 isotope data. *Water Resour. Res.* 5, 2–2. <https://doi.org/10.1111/j.1752-1688.1969.tb04897.x>
- 914 Siderius, C., Biemans, H., Wiltshire, A., Rao, S., Franssen, W. H. P., Kumar, P., Gosain, A. K., Vliet, M.
915 T. H. Van, Collins, D. N., 2013. Science of the Total Environment Snowmelt contributions to
916 discharge of the Ganges. *Sci. Total Environ.* 468–469, S93–S101.
917 <https://doi.org/10.1016/j.scitotenv.2013.05.084>
- 918 Sprenger, M., Stumpp, C., Weiler, M., Aeschbach, W., & Werner, C. (2019). The demographics of
919 water: a review of water ages in the critical zone. *Reviews of Geophysics*.
- 920 Stadnyk, T. A., & Holmes, T. L. (2020). On the value of isotope-enabled hydrological model
921 calibration. *Hydrological Sciences Journal*, 1-14.
- 922 Stewart, M. K., Morgenstern, U., & McDonnell, J. J. (2010). Truncation of stream residence time: how
923 the use of stable isotopes has skewed our concept of streamwater age and origin. *Hydrological*
924 *Processes*, 24(12), 1646-1659.
- 925 Terzer, S., Wassenaar, L. I., Araguás-Araguás, L. J., & Aggarwal, P. K. (2013). Global isoscapes for $\delta^{18}\text{O}$
926 and $\delta^2\text{H}$ in precipitation: improved prediction using regionalized climatic regression
927 models. *Hydrology and Earth System Sciences*, 17(11), 4713-4728.
- 928 Tetzlaff, D., Birkel, C., Dick, J., Geris, J., & Soulsby, C. (2014). Storage dynamics in hydrogeological
929 units control hillslope connectivity, runoff generation, and the evolution of catchment transit time
930 distributions. *Water Resources Research*.
- 931 The newest report from the second scientific expedition to Tibetan Plateau, 2018.
932 (<http://energy.people.com.cn/n1/2018/0910/c71661-30281998.html>).
- 933 Tian, F., Hu, H., Lei, Z., & Sivapalan, M. (2006). Extension of the Representative Elementary Watershed
934 approach for cold regions via explicit treatment of energy related processes.
- 935 Tian, F., Li, H., & Sivapalan, M. (2012). Model diagnostic analysis of seasonal switching of runoff
936 generation mechanisms in the Blue River basin, Oklahoma. *Journal of Hydrology*, 418, 136-149.
- 937 Tian F., Xu R., Nan Y., Li K., He Z. (2020) Quantification of runoff components in the Yarlung
938 Tsangpo River using a distributed hydrological model. *Advances in Water Science*, 31(3): 324-336.
- 939 [Tong, R., Parajka, J., Salentinig, A., Pfeil, I., Komma, J., Széles, B., Kubáň, M., Valent, P., Vreugdenhil,](#)

- 940 [M., Wagner, W., and Blöschl, G.: The value of ASCAT soil moisture and MODIS snow cover data for](#)
941 [calibrating a conceptual hydrologic model, *Hydrol. Earth Syst. Sci.*, 25, 1389–1410,](#)
942 [https://doi.org/10.5194/hess-25-1389-2021, 2021.](https://doi.org/10.5194/hess-25-1389-2021)
- 943 van der Velde, Y., Heidbüchel, I., Lyon, S. W., Nyberg, L., Rodhe, A., Bishop, K., & Troch, P. A. (2015).
944 Consequences of mixing assumptions for time - variable travel time distributions. *Hydrological*
945 *Processes*, 29(16), 3460-3474.
- 946 van Huijgevoort, M. H. J., Tetzlaff, D., Sutanudjaja, E. H., & Soulsby, C. (2016). Using high resolution
947 tracer data to constrain water storage, flux and age estimates in a spatially distributed rainfall-runoff
948 model. *Hydrological Processes*, 30(25), 4761-4778.
- 949 [Wang, L., Niu, S., Good, S. P., Soderberg, K., McCabe, M. F., Sherry, R. A., ... & Caylor, K. K. \(2013\).](#)
950 [The effect of warming on grassland evapotranspiration partitioning using laser-based isotope](#)
951 [monitoring techniques. *Geochimica et Cosmochimica Acta*, 111, 28-38.](#)
- 952 Weiler, M., Seibert, J., Stahl, K., 2018. Magic components — why quantifying rain , snowmelt , and
953 icemelt in river discharge is not easy. *Hydrol. Process.* 32, <https://doi.org/10.1002/hyp.11361>
- 954 Wilusz, D. C., Harman, C. J., & Ball, W. P. (2017). Sensitivity of catchment transit times to rainfall
955 variability under present and future climates. *Water Resources Research*, 53(12), 10231-10256.
- 956 Wolfe, B. B., Karst-Riddoch, T. L., Hall, R. I., Edwards, T. W., English, M. C., Palmini, R., ... & Vardy,
957 S. R. (2007). Classification of hydrological regimes of northern floodplain basins (Peace–Athabasca
958 Delta, Canada) from analysis of stable isotopes ($\delta^{18}\text{O}$, $\delta^2\text{H}$) and water chemistry. *Hydrological*
959 *Processes: An International Journal*, 21(2), 151-168.
- 960 [Xi, X. \(2014\). A review of water isotopes in atmospheric general circulation models: recent advances](#)
961 [and future prospects. *International Journal of Atmospheric Sciences*, 2014.](#)
- 962 Xu, R., Hu, H., Tian, F., Li, C., & Khan, M. Y. A. (2019). Projected climate change impacts on future
963 streamflow of the Yarlung Tsangpo-Brahmaputra River. *Global and Planetary Change*, 175, 144-159.
- 964 Yang, L., Tian, F., Sun, Y., Yuan, X., & Hu, H. (2014). Attribution of hydrologic forecast uncertainty
965 within scalable forecast windows. *Hydrology and Earth System Sciences*, 18(2), 775.
- 966 Yao, T. , Thompson, L. , Yang, W. , Yu, W. , Gao, Y. , & Guo, X. , et al. (2012). Different glacier status
967 with atmospheric circulations in tibetan plateau and surroundings. *Nature Climate Change*, 2.
- 968 Yin, C., Tian, L., Yu W. & Gong T. (2006). Variations of stable oxygen isotope in precipitation in the
969 Basin of Yamzho Lake. *Journal of Glaciology and Geocryology*, 28(6), 918-924.
- 970 Zhang F. , Li J. , & Gong T. (2006). Hydrological regime of the Karuxung watershed in north
971 Himalayas. *Acta Geographica Sinica*, 61(11), 1141-1148.
- 972 Zhang, F., Zhang, H., Hagen, S. C., Ye, M., Wang, D., Gui, D., ... & Liu, J. (2015). Snow cover and runoff
973 modelling in a high mountain catchment with scarce data: effects of temperature and precipitation

974 parameters. Hydrological processes, 29(1), 52-65.

975 Zhang, L., Su, F., Yang, D., Hao, Z., & Tong, K. (2013). Discharge regime and simulation for the
976 upstream of major rivers over Tibetan Plateau. Journal of Geophysical Research:
977 Atmospheres, 118(15), 8500-8518.

978 [Zhao, L., Xiao, H., Zhou, M., Cheng, G., Wang, L., Yin, L., & Ren, J. \(2012\). Factors controlling spatial
979 and seasonal distributions of precipitation \$\delta^{18}O\$ in China. Hydrological Processes, 26\(1\), 143-152.](#)

980 Zongxing, L. , Qi, F. , Zongjie, L. , Ruifeng, Y. , Juan, G. , & Yuemin, L. . (2019). Climate background,
981 fact and hydrological effect of multiphase water transformation in cold regions of the western china:
982 a review. EARTH ENCE REVIEWS.

983

984

List of figures

985

1. **Figure 1.** Location and topography of the study area

986

2. **Figure 2.** Uncertainty ranges of simulations in the calibration period produced by the behavioral parameter sets of the single-objective (subfigure a to c), dual-objective (subfigure d to f) and triple-objective (subfigure g to i) calibration variants.

987

988

989

3. **Figure 3.** Daily simulations of (a) each water source and (b) the corresponding isotopic compositions. The black points and red/blue lines in subfigure (b) mean the isotope composition of the water sources as represented by the corresponding color in subfigure (a).

990

991

992

4. **Figure 4.** Average proportion of different sources in the annual water input for runoff generation

993

5. **Figure 5.** Seasonal contributions of rainfall, snowmelt and glacier melt to total water input estimated by the (a) single-objective, (b) dual-objective and (c) triple-objective calibration variants. The error bars indicate the uncertainty ranges simulated by the corresponding behavior parameter sets.

994

995

996

6. **Figure 6.** Comparison between the MM and FT methods: scatterplots for daily (a) MTT and (d) MRT; time series of the daily (b) MTT and (e) MRT; and probability density functions of the daily (c) MTT and (f) MRT.

997

998

999

7. **Figure 7.** Uncertainty ranges of time series (a) MTT and (b) MRT simulated by MM method.

1000

8. **Figure 8.** The weighted average probability distributions of (a) forward TTD, (b) backward TTD, and (c) RTD estimated by FT method.

1001

1002

9. **Figure 9.** The role of isotope calibration on constraining the proportion of runoff components. (a) The relationship between MAE_{iso} and proportion of glacier melt. (b) The relationship between MAE_{iso} and proportion of surface runoff. (c) The relationship between proportion of surface runoff and that of glacier melt. (d) The simulated isotope in stream water produced by the parameter sets estimating proportion of glacier melt higher than 40%. (e) The simulated isotope in stream water produced by the parameter sets estimating proportion of surface runoff lower than 45%.

1003

1004

1005

1006

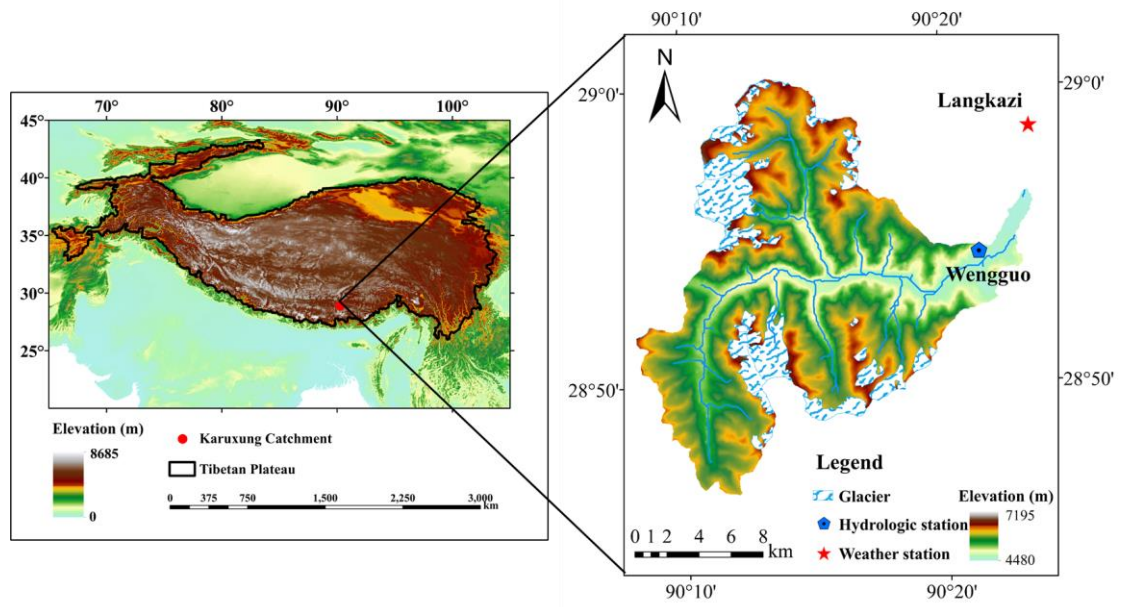
1007

1008

9,10. **Figure 10.** The scatter diagrams between (a) MRT and soil water content, (b) backward MTT and soil water content, (c) backward MTT and rainfall, and (d) forward MTT and temperature.

1009

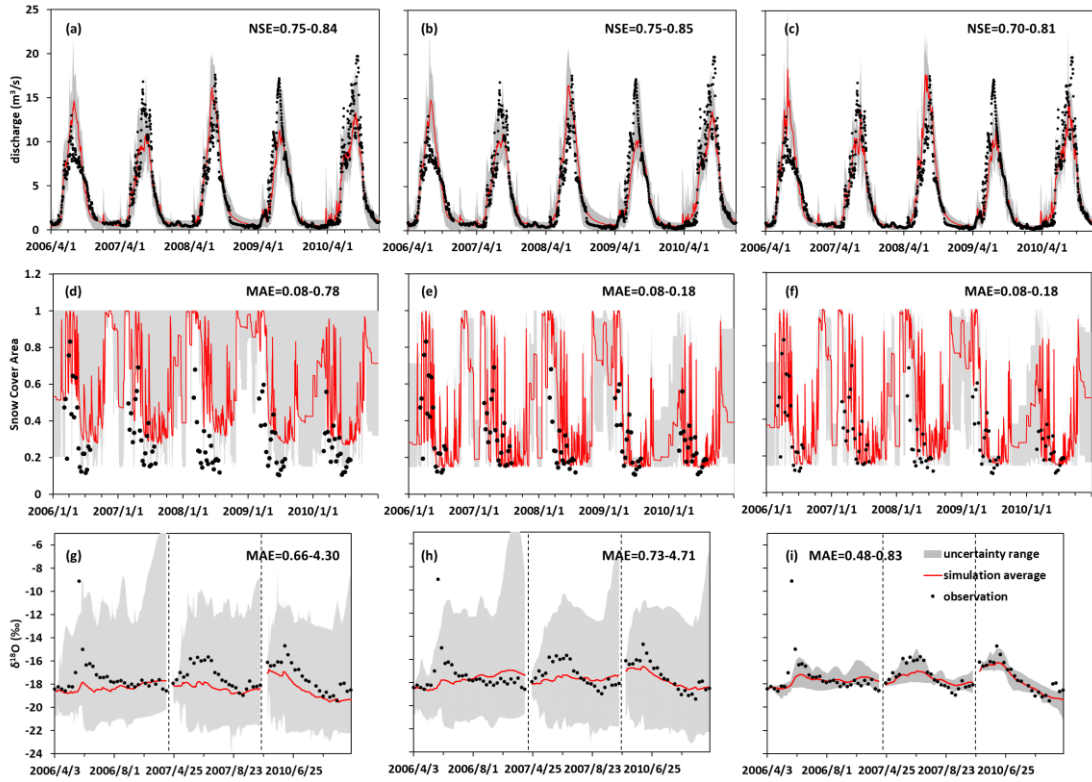
1010



1011

1012 **Figure 1.** Location and topography of the study area

1013



1014

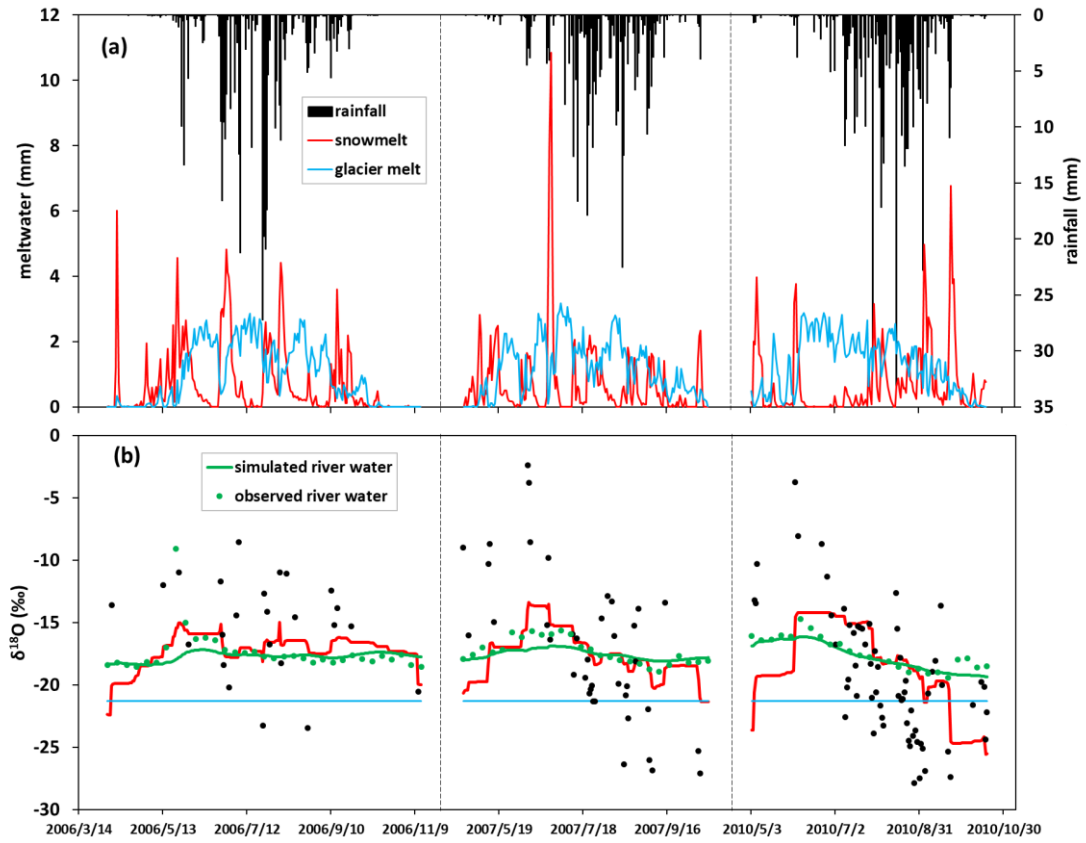
1015

1016

1017

1018

Figure 2. Uncertainty ranges of simulations in the calibration period produced by the behavioral parameter sets of the single-objective (subfigure a to c), dual-objective (subfigure d to f) and triple-objective (subfigure g to i) calibration variants.



1019

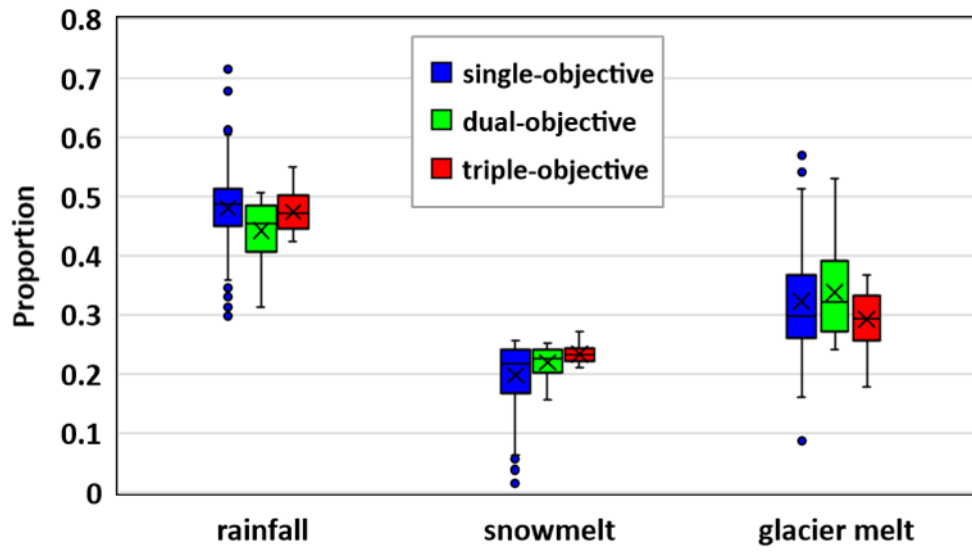
1020

1021

1022

1023

Figure 3. Daily simulations of (a) each water source and (b) the corresponding isotopic compositions. The black points and red/blue lines in subfigure (b) represent the isotope composition of the water sources as represented by the corresponding color in subfigure (a).

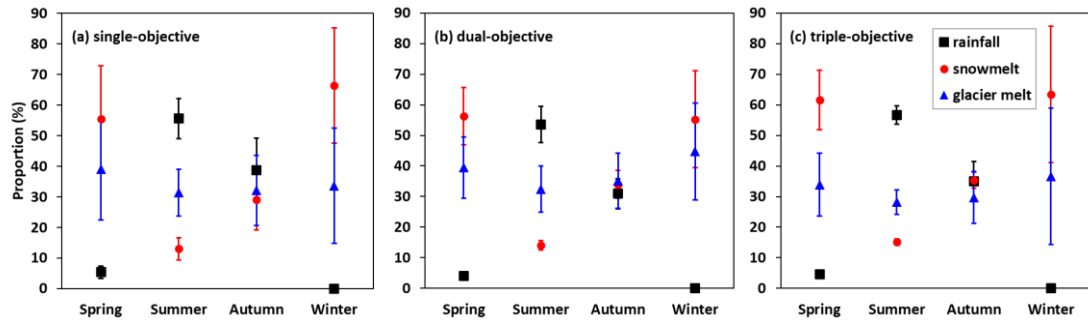


1024

1025

Figure 4. Average proportion of different sources in the annual water input for runoff generation

1026



1027

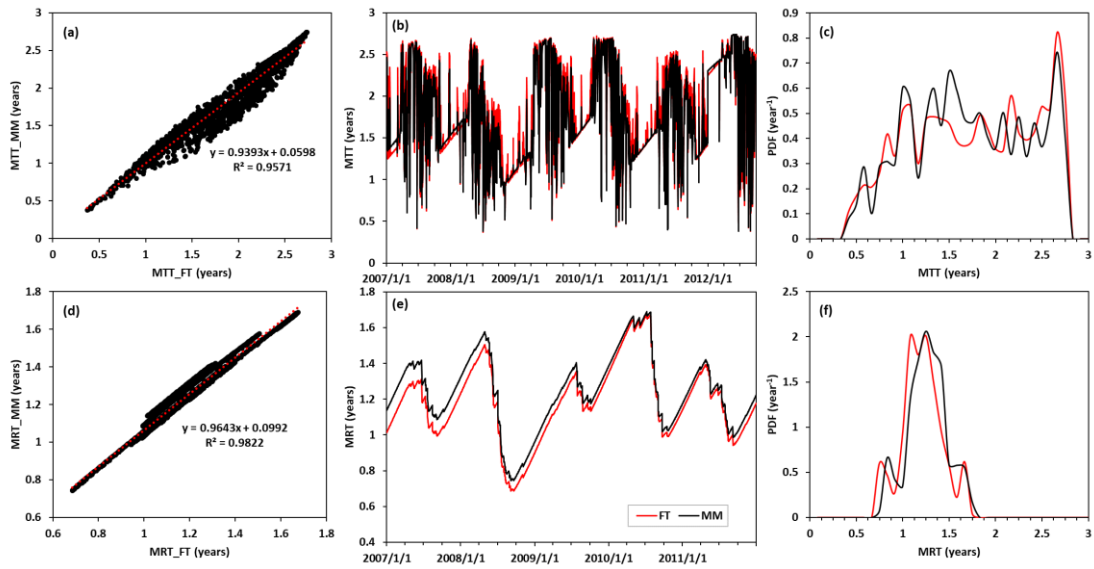
1028

1029

1030

1031

Figure 5. Seasonal contributions of rainfall, snowmelt and glacier melt to total water input estimated by the (a) single-objective, (b) dual-objective and (c) triple-objective calibration variants. The error bars indicate the uncertainty ranges simulated by the corresponding behavior parameter sets.



1032

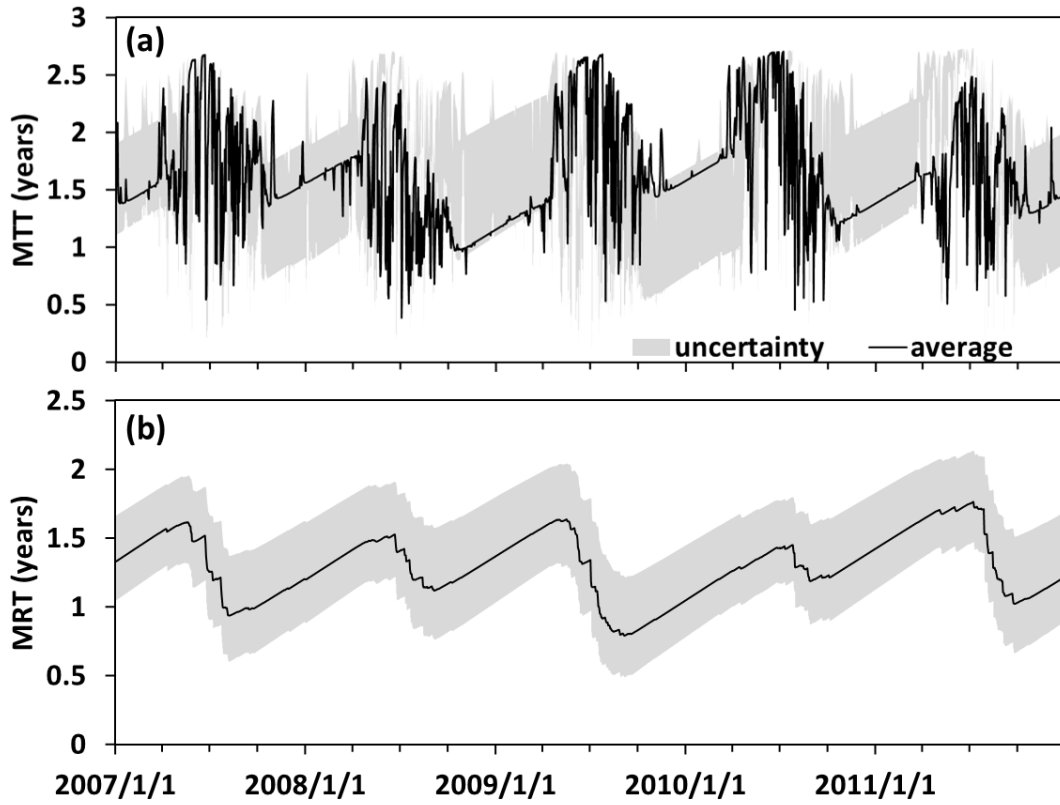
1033

1034

1035

1036

Figure 6. Comparison between the MM and FT methods: scatterplots for daily (a) MTT and (d) MRT; time series of the daily (b) MTT and (e) MRT; and probability density functions of the daily (c) MTT and (f) MRT.

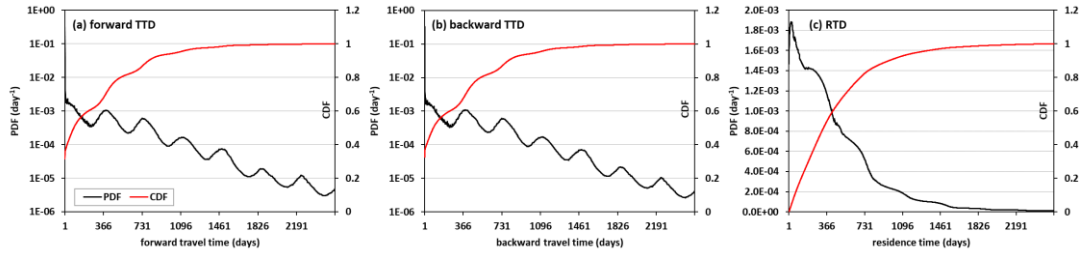


1037

1038

1039

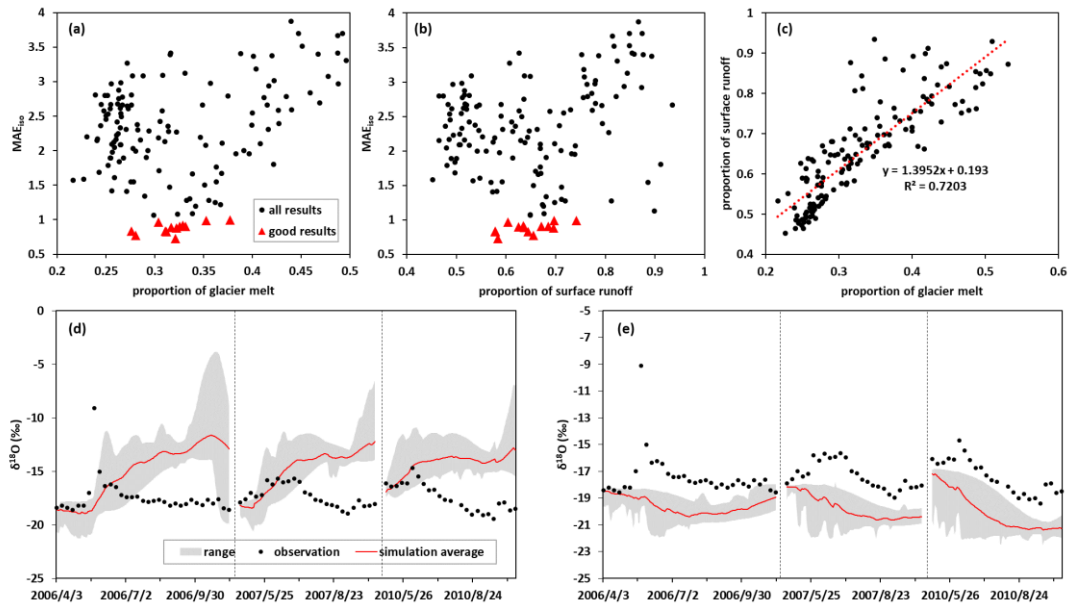
Figure 7. Uncertainty ranges of time series (a) MTT and (b) MRT simulated by MM method.



1040

1041 **Figure 8.** The weighted average probability distributions of (a) forward TTD, (b) backward TTD, and (c)
 1042 RTD estimated by FT method

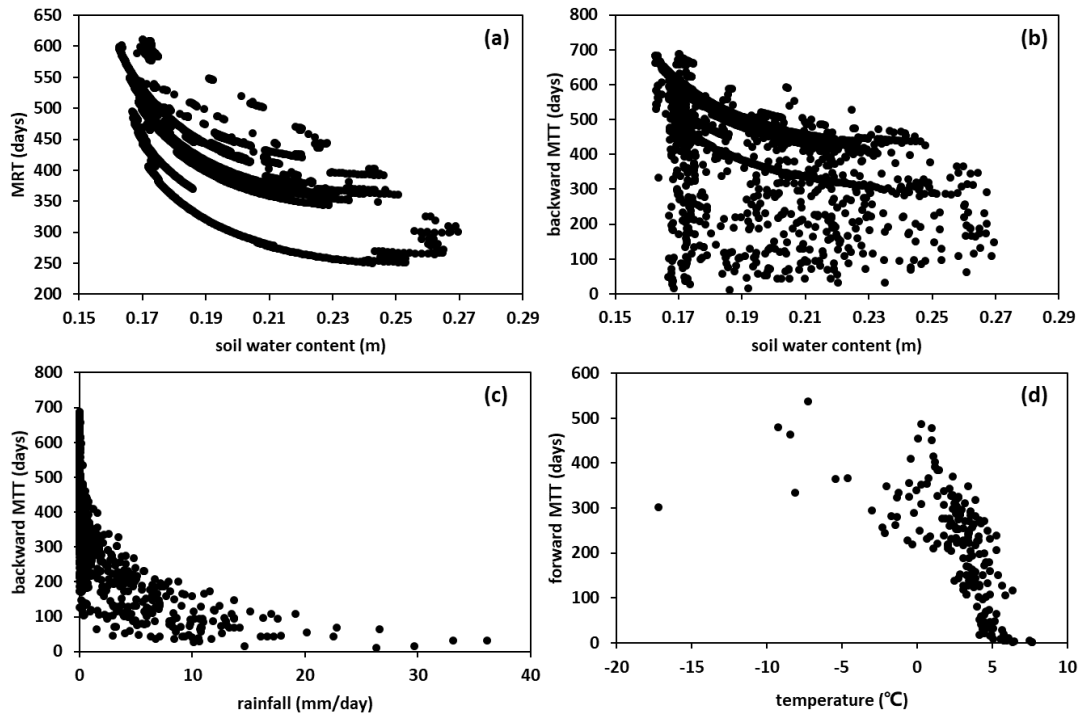
1043



1044

1045 **Figure 9.** The role of isotope calibration on constraining the proportion of runoff components. (a) The
 1046 relationship between MAE_{iso} and proportion of glacier melt. (b) The relationship between MAE_{iso} and
 1047 proportion of surface runoff. (c) The relationship between proportion of surface runoff and that of glacier
 1048 melt. (d) The simulated isotope in stream water produced by the parameter sets estimating proportion of
 1049 glacier melt higher than 40%. (e) The simulated isotope in stream water produced by the parameter sets
 1050 estimating proportion of surface runoff lower than 45%.

1051



1052

1053

1054

1055

1056

Figure 10. The scatter diagrams between (a) MRT and soil water content, (b) backward MTT and soil water content, (c) backward MTT and rainfall, and (d) forward MTT and temperature.

1057

List of tables

- 1058 1. **Table 1.** Characteristics of the precipitation and stream water samples
- 1059 2. **Table 2.** Calibrated parameters of the THREW-t model
- 1060 3. **Table 3.** Comparisons of the model performance produced by three calibration variants.
- 1061 4. **Table 4.** Average percentages of water sources in the annual water input for runoff generation.
- 1062 5. **Table 5.** Simulated contributions of runoff components to annual runoff
- 1063

1064 **Table 1.** Characteristics of precipitation and stream samples

Year	Period	Precipitation sample number	Stream sample number
2006	April 6 th to November 11 th	24	31
2007	April 23 rd to October 9 th	39	25
2010	May 5 th to October 18 th	63	23
2011	March 28 th to November 6 th	69	32
2012	June 16 th to September 22 nd	42	14

1065

1066

1067

Table 2. Calibrated parameters of the THREW-t model

Symbol	Unit	Physical descriptions	Range
nt	-	Manning roughness coefficient for hillslope	0-0.2
WM	cm	Tension water storage capacity, used in Xinanjiang model (Zhao, 1992) to calculate saturation area	0-10
B	-	Shape coefficient used in Xinanjiang model to calculate saturation area	0-1
KKA	-	Coefficient to calculate subsurface runoff in $Rg=KKD \cdot S \cdot K_S^S \cdot (y_s/Z)^{KKA}$, where S is the topographic slope, K_S^S is the saturated hydraulic conductivity, y_s is the depth of saturated groundwater, Z is the total soil depth	0-6
KKD	-	See description for KKA	0-0.5
T_0	°C	Melting threshold temperature used in Eqs. (1) and (2)	-5-5
DDF_{SN}	mm/°C/day	Degree day factor for snow	0-10
DDF_G	mm/°C/day	Degree day factor for glacier	0-10
CI	-	Coefficient to calculate the runoff concentration process using Muskingum method: $O_2=C_1 \cdot I_1+C_2 \cdot I_2+C_3 \cdot O_1+C_4 \cdot Q_{lat}$, where I_1 and O_1 is the inflow and outflow at prior step, I_2 and O_2 is the inflow and outflow at current step, Q_{lat} is lateral flow of the river channel, $C_3=1-C_1-C_2$, $C_4=C_1+C_2$	0-1
$C2$	-	See description for CI	0-1

1068

1069

1070

Table 3. Comparisons of the model performance produced by three calibration variants.

calibration variant	Number of behavior parameter sets	period	NSE_{dis}^a	MAE_{SCA}	MAE_{iso}
Single-objective	126	calibration	0.79 (0.75-0.84)	0.25 (0.08-0.78)	2.21 (0.66-4.10)
		validation	0.79 (0.71-0.84)	0.24 (0.07-0.79)	2.53 (0.77-4.88)
Dual-objective	117	calibration	0.79 (0.75-0.85)	0.10 (0.08-0.18)	2.18 (0.73-4.71)
		validation	0.80 (0.73-0.84)	0.08 (0.06-0.19)	2.38 (0.84-4.96)
Triple-objective	19	calibration	0.74 (0.70-0.81)	0.13 (0.08-0.18)	0.68 (0.48-0.83)
		validation	0.79 (0.73-0.84)	0.11 (0.06-0.18)	0.93 (0.72-1.19)

1071

a: Bracketed values represent the minimal and maximal values produced by the behavioral parameter sets.

1072

1073

1074 **Table 4.** Average percentages of water sources in the annual water input for runoff
 1075 generation.

Season	Water source ^a	Single-objective	Dual-objective	Triple-objective
Annual	Rainfall	48.0	44.2	47.4
	Snow melt	19.7	22.0	23.4
	Glacier melt	32.2	33.8	29.2
	Uncertainty	12.4	9.4	6.2
Spring	Rainfall	5.4	4.1	4.5
	Snow melt	55.5	56.3	61.6
	Glacier melt	39.1	39.5	33.9
	Uncertainty	24.2	13.7	14.2
Summer	Rainfall	55.6	53.5	56.6
	Snow melt	13.0	14.0	15.2
	Glacier melt	31.4	32.4	28.2
	Uncertainty	10.7	9.7	5.1
Autumn	Rainfall	38.7	30.9	35.0
	Snow melt	29.2	33.9	35.3
	Glacier melt	33.6	35.1	29.7
	Uncertainty	18.5	11.2	11.0
Winter	Rainfall	0	0	0
	Snow melt	66.4	55.3	63.3
	Glacier melt	33.6	44.7	36.7
	Uncertainty	26.6	22.3	31.5

1076 a: The uncertainty of the contribution is defined as $E = \sqrt{E_R^2 + E_S^2 + E_G^2}$, where E_R , E_N and E_G
 1077 represent the standard deviations of the contributions of the water sources produced by the corresponding
 1078 behavioral parameter sets. Subscripts of R , S and G represent rainfall, snow meltwater and glacier
 1079 meltwater, respectively.

1080
 1081

Table 5. Simulated contributions of runoff components to annual runoff

Season	Runoff path	Single-objective	Dual-objective	Triple-objective
Annual	Surface	65.9	66.4	64.9
	Subsurface	34.1	33.6	35.1
	Uncertainty	11.8	12.1	4.1
Spring	Surface	64.3	64.0	68.0
	Subsurface	35.7	36.0	32.0
	Uncertainty	10.4	9.2	7.2
Summer	Surface	79.9	79.0	79.1
	Subsurface	20.1	21.0	20.9
	Uncertainty	10.0	10.7	4.4
Autumn	Surface	40.1	43.1	36.6
	Subsurface	59.9	56.9	63.4
	Uncertainty	15.4	16.0	6.7
Winter	Surface	5.1	5.0	5.0
	Subsurface	94.9	95.0	95.0
	Uncertainty	9.9	4.5	2.7